Reducing Hydrological Uncertainty in Large Mountainous Basins: The Role of Isotope, Snow Cover, and Glacier Dynamics in Capturing Streamflow Seasonality

Diego Avesani¹, Yi Nan², and Fuqiang Tian^{2,3}

Correspondence: Yi Nan (ny1209@qq.com)

Abstract. Hydrological modeling in large mountainous catchments faces challenges due to the complex interplay of snowmelt, glacier dynamics, and groundwater contributions, which introduce significant uncertainty in streamflow predictions. This study introduces a Bayesian multi-objective parameter estimation framework to reduce predictive streamflow uncertainty in large mountainous catchments by integrating streamflow likelihood with three auxiliary likelihoods, analyzed individually: snow cover area (SCA), glacier mass balance (GMB), and isotopic composition (I). The well-established Generalized Likelihood Uncertainty Estimation (GLUE) method is employed to investigate trade-offs among these likelihoods, providing a detailed assessment of their distinct and combined contributions to hydrological model performance across various flow regimes. The semi-distributed Representative Elementary Watershed-Tracer aided version (THREW-T) hydrological model applied in this work captures both rapid surface dynamics and slow-response subsurface processes, offering a comprehensive representation of streamflow variability.

Results indicate that isotopic likelihood plays a critical role in reducing low-flow uncertainty by effectively constraining baseflow subsurface flow and groundwater-surface water interactions, particularly during winter and early spring when these processes dominate. Conversely, while SCA and GMB likelihoods demonstrate some effectiveness in capturing rapid processes such as snowmelt and glacier melt, their influence is most pronounced during the melting season, with limited impact on reducing overall streamflow uncertainty. This seasonality is reflected in sharpness values, which measure how much uncertainty is reduced, with isotopic likelihood achieving the highest peak of 0.34 in late winter, whereas SCA and GMB reach maximum sharpness values of 0.19 and 0.16, respectively, during the melting season. Pareto plots further reveal the synergies and trade-offs associated with each likelihood, underscoring the importance of adopting a multi-objective calibration approach that accounts for seasonal variations in hydrological processes. In addition, the results highlight the critical role of seasonality in shaping the effectiveness of auxiliary likelihoods, emphasizing their potential to improve predictive accuracy and reduce uncertainty in hydrological models.

Copyright statement. TEXT

¹Department of Civil, Environmental and Mechanical Engineering, University of Trento, 38123 Trento, Italy

²State Key Laboratory of Hydroscience and Engineering, Tsinghua University, Beijing 100084, China

³Department of Hydraulic Engineering, Tsinghua University, Beijing 100084, China

1 Introduction

30

35

40

Accurate hydrological modeling in large mountainous catchments remains particularly challenging due to the inherent complexity of these systems (Gupta et al., 2008). The interplay of multiple water sources, such as snowmelt, glacier dynamics, and groundwater, combined with substantial spatio-temporal variability in streamflow generation, often results in equifinality and significant uncertainty in predictions (e.g., Asong et al., 2020; Shuai et al., 2022; Dalla Torre et al., 2024). These complexities call for advanced modeling approaches capable of improving our understanding of streamflow variability and supporting effective water resource management (Panchanathan et al., 2024).

Recent advancements in hydrological modeling have addressed these demands by focusing on the integration of auxiliary variables, such as snow cover area, glacier mass balance, and environmental tracers (e.g., stable oxygen isotopes, $\delta^{18}O$), to improve model calibration and reduce parameter uncertainty (Di Marco et al., 2021; Nan et al., 2021b; Mohammadi et al., 2023). These variables provide critical insights into cryospheric and subsurface processes, enabling models to better capture hydrological responses that drive streamflow variability during periods of low flow (Panchanathan et al., 2024). Incorporating such data improves the representation of specific model components and guides the evaluation of the model, ultimately enhancing reliability and reducing equifinality (Birkel et al., 2014; Tetzlaff et al., 2014). Tracer-aided modeling has proven particularly effective in disentangling hydrological processes and identifying critical contributions from snowmelt and groundwater under varying conditions (Nan et al., 2021b). Bayesian approaches have also been applied to explicitly address equifinality and uncertainty in hydrological modeling in various mountain basins (e.g., Yang et al., 2007; Andraos, 2024).

Nonetheless, several challenges remain. Few studies have systematically compared the relative effectiveness of auxiliary datasets - such as snow cover area, glacier mass balance, and isotopic tracers - in reducing model uncertainty and equifinality across different flow regimes (Finger et al., 2011; Xu et al., 2012; Nan and Tian, 2024). While some studies have explored the role of individual datasets, such as isotopic tracers (Nan and Tian, 2024) or glacier mass balance (Finger et al., 2011), a unified comparison of their respective contributions within a single modeling framework remains absent. This is particularly true for low-flow conditions, which are often dominated by slow-response processes such as groundwater contributions and subsurface flow dynamics (Betterle and Bellin, 2024). Moreover, the potential for these datasets to improve the representation of hydrological processes under varying seasonal conditions remains largely unexplored. Similarly, while previous work has explored the Contributions of Runoff Components (CRC) to total streamflow (e.g., subsurface flow, rainfall runoff, snowmelt, and glacier melt) (Stahl et al., 2008), a comprehensive understanding of how these components interact to influence streamflow dynamics under different conditions remains insufficiently constrained by multi-source datasets. Current Bayesian frameworks, while powerful, often fail to fully leverage the complementary strengths of auxiliary datasets, particularly in large mountainous catchments where complex cryospheric and subsurface interactions drive streamflow dynamics (Zhang et al., 2018; Chang et al., 2024).

This study addresses these gaps by systematically evaluating the role of snow cover area, glacier mass balance, and isotopic tracers in reducing model uncertainty and equifinality within a fully Bayesian framework. The analysis is applied to Focusing on the Yarlung Tsangpo River Basin,—a large mountainous catchment characterized by complex cryospheric and

subsurface interactions, where streamflow variability is influenced by arises from snowmelt, glacier dynamics, and groundwater contributions. Specifically, we aim to investigate the complementary roles of we investigate how these auxiliary datasets can complement each other in constraining hydrological models and improving the understanding of streamflow variability across different flow regimes. Special emphasis is placed on low-flow periods, during which isotopic data have proven to be particularly effective in reducing uncertainty by providing stronger constraints on baseflow contributions and groundwater-surface provide particularly strong constraints on subsurface flow and groundwater-surface water interactions (Rodgers et al., 2005). The study explores how By adopting a multi-source calibration approaches can address uncertainty and approach, we explore trade-offs in model performance across various hydrological conditions. Additionally, this work aims to quantify the influence of each dataset on and quantify how each dataset influences the contributions of runoff components, shedding light on the interplay between subsurface flowsnowmelt, glacier melt, rainfall runoff, snowmelt, and glacier melt in total streamflow generation. By analyzing how different datasets affect these runoff components, the study seeks to enhance the representation of hydrological processes and improve our understanding of how various sources contribute to streamflow variability. These insights will be particularly relevant for water resource and subsurface flow. By shedding light on streamflow generation processes, particularly during low-flow periods, these findings may offer a first step toward more integrated and nuanced water management strategies in mountainous regions, where low-flow dynamics are critical for drought mitigation (Wu et al., 2023) and the long-term sustainability of water resources (Haro-Monteagudo et al., 2020) complex mountainous regions facing increasing drought risk (Wu et al., 2023).

To address these objectives, the paper is organized as follows: the adopted tracer-aided hydrological model, the study area, and the Bayesian framework are described in Sect. 2. Sect. Section 2. Section 3 presents the results, including parameter distributions, uncertainty analysis, and flow regime-specific improvements. Sect. Section 4 discusses the implications of the findings, while Sect. Section 5 provides concluding remarks and future research directions.

2 Materials and methods

70

2.1 Study area and data

The Yarlung Tsangpo River (YTR) basin was selected as the focus area of this study (Figure 2). The YTR basin is the upstream part of the Brahamaputra River basin, located on the southern Tibetan Plateau (TP). The YTR basin, as one of the longest rivers originating from the TP, extends in the range of 27-32°N and 82-97°E with an elevation extent of 2900-6900 m above sea level. The outlet hydrological station of the YTR basin is the Nuxia station, with a drainage area of approximately $2 \times 10^5 \, \text{km}^2 2 \times 10^5 \, \text{km}^2$. There are four hydrological stations along the mainstream of YTR: Nuxia, Yangcun, Nugesha and Lazi, from downstream to upstream . The (Table 1). During 1990-2015, the mean annual precipitation in the YTR basin is around 500-490 mm, which is dominated by the South Asian monsoon in the Indian Ocean hydrosphere-atmosphere system resulting an obvious wet season during June to September. The mean annual temperature is -0.2-1.5°C, leading to widely distributed snow and glacier, covering around 16.3% and 1.5% of the basin.

Datasets of meteorological input, topography, underlying surface, streamflow and isotope were collected to establish the model. The 30 m resolution digital elevation model (DEM) were downloaded from the Geospatial Data Cloud (https://www.gscloud.cn) for simulation unit dividing. Daily precipitation and temperature were extracted from the 0.1° China Meteorological Forcing Dataset (CMFD, Yang and He (2019)) (Yang and He, 2019), which was produced by merging multiple satellite datasets with the national meteorological station data. The daily potential evapotranspiration were obtained from the 1.0° reanalysis dataset ERA5 Land (Muñoz-Sabater et al., (2021)) (Muñoz-Sabater et al., 2021). For the underlying conditions, the MODIS leaf area index (LAI) product MOD15A2H (Myneni et al., (2015)) (Myneni et al., 2015) and the normalized difference vegetation index (NDVI) product MOD13A3 (Didan (2015)) (Didan, 2015) were used to represent the vegetation conditions and determine the ratio of vegetation covered area, and the Marmonized World Soil Database (HWSD, He (2019)) (He, 2019) was used to estimate the soil property parameters not obtained by model calibration (including saturated hydraulic conductivity, soil porosity, soil pore distribution index, field capacity, and air entry value). For the cryospheric elements, the Tibetan Plateau Snow Cover Extent (TPSCE) product (Chen et al. (2018)) and the second glacier inventory dataset of China (Liu (2012)) were adopted to denote the snow and glacier cover areas. The (Liu, 2012) was adopted to determine the boundary of regions where glacier simulation should be performed. The daily Tibetan Plateau Snow Cover Extent (TPSCE) product (Chen et al., 2018) during 2001-2015 and the 0.5° yearly glacier elevation change data dataset developed by Hugonnet et al. (2021) was during 2001-2010 were used to validate the simulated snow cover area (SCA) and glacier mass balance (GMB). Daily streamflow observation data at the Nuxia, Yangcun, and Nugesha stations were collected to evaluate the performance of the hydrological simulations. However, due to Chinese national regulations, streamflow data for the Yarlung Tsangpo River—a transboundary river system—are considered sensitive and classified as confidential. As such, these data cannot be publicly disclosed or shared in this publication. This restriction reflects broader geopolitical concerns, as highlighted by Lin et al. (2023), who emphasize the particular sensitivity of hydrological data in transboundary basins and regions subject to resource and geopolitical tensions. Considering the availability period of the supporting datasets, the simulation period was set from 2001.01.01 to 2015.12.31, aligned with the time span of the meteorological and vegetation input data.

100

105

115

120

Grab samples of stream and precipitation water were collected in 2005 at four stations to analyze the isotope composition ($\delta^{18}O$) to validate the tracer simulation (Table 1). The outputs of the Scripps Global Spectral Model with an isotope incorporated (isoGSM, Yoshimura et al. (2008)) with 1.875° resolution were extracted to represent the spatiotemporal variation of the isotope composition in precipitation. The bias assessment and correction procedure was conducted based on measurement precipitation isotope data in our previous work, Our previous evaluation on isoGSM (Nan et al., 2021a) indicated that it can effectively capture the seasonal variation in precipitation $\delta^{18}O$, but exhibited a systematic overestimation bias in the study region and performed relatively poorly in accurately capturing the isotope signature of specific events (Supplementary Figures S1 and the corrected isoGSM S2). The bias corrected isoGSM product produced by Nan et al. (2022) was adopted as the input data, in which the bias of isoGSM was adjusted based on a linear regression with altitude. Rainfall and snowfall were assumed to have the same isotope composition as the precipitation $\delta^{18}O$ is assumed to be temporally constant and 5% lower

than the weighted average of local precipitation $\delta^{18}O$. The value of the offset parameter was estimated from the data collected by Boral and Sen (2020).

Table 1. Data and sample information at four hydrological stations adopted

Station	Coordinate	Elevation (m)	Streamflow	Isotope				
			Period	Period (in 2005)	Precipitation		Stream water	
					number of samples	$\underbrace{\delta^{18}_{\sim}}\underbrace{O}_{\sim}(\%)$	number of samples	$\delta^{18}_{\sim} O(\%)$
Nuxia	94.65°E, 29.47°N	<u>3691</u>	2001–2015	14 Mar-23 Oct	<u>86</u>	-10.33	$\stackrel{34}{\sim}$	-15.74
Yangcun	91.82°E, 29.27°N	<u>4541</u>	2001-2010	17 Mar-5 Oct	<u>59</u>	-13.14	<u>30</u>	-16.57
Nugesha	89.71°E, 29.32°N	<u>4715</u>	2001-2010	14 May–22 Oct	45 ≈	-14.29	25 ≈	-17.84
<u>Lazi</u>	87.58°E, 29.12°N	<u>4889</u>	/	6 Jun-22 Sep	42	-17.41	22	-16.52

2.2 The tracer-aided hydrological model

125

140

145

A distributed semi-distributed tracer-aided cryospheric-hydrological model, Tsinghua Representative Elementary Watershed-Tracer aided version (THREW-T) developed by Tian et al. (2006) and Nan et al. (2021b) was adopted to simulate the hydrological, cryospheric and isotopic processes in the YTR basin (Figure 1). The THREW-T model uses the representative watershed method (REW) for spatial discretization, which divides the whole catchment into REWs based on DEM data. Two vertical layers including eight subzones (i.e., surface layer including vegetation zone, bare zonesoil, sub-stream network zone, snow-covered zone, glacier-covered zone and main channel reach zone; subsurface layer including unsaturated zone and saturated zone) are defined for each REW-based on the underlying surface type. The YTR basin was divided into 297 REWs with average area of 694 km² km² in this study. The areal averages of the gridded datasets were calculated for each REW, which were used as the input for simulation. More detailed descriptions of REW method could be found in Reggiani et al. (1999) and Tian et al. (2006).

The cryospheric module was incorporated into the model to simulate the evolutions of snowpack and glacier. The total precipitation was partitioned into liquid (rainfall) and solid precipitation (snowfall), according to a temperature threshold set as 0°C0°C. For the simulation of snowpack, the snow water equivalent of each REW was updated based on the snowfall and the snowmelt, which was calculated using the degree-day factor method. The snow cover area (SCA) was determined by the snow cover depletion curve (Fassnacht et al. (2016)) (Fassnacht et al., 2016) and then compared with the satellite observation data. The snow sublimation was not simulated in the model, because previous studies estimated that the sublimation losses in the study region only accounted for 2 3% of the annual snowfall, as the results of the wet climate condition (Khanal et al., 2021; Sun et al., 2024; Lutz et al., 2016). For the simulation of glacier, each REW was further divided into several elevation bands with an interval of 200m, to represent the variation in temperature and precipitation along the altitudinal profile. The glacier within the intersection of each REW and elevation band was regarded as the representative unit for glacier simulation. The processes related to glacier evolution in the model included the snow accumulation and snowmelt over glaciers,

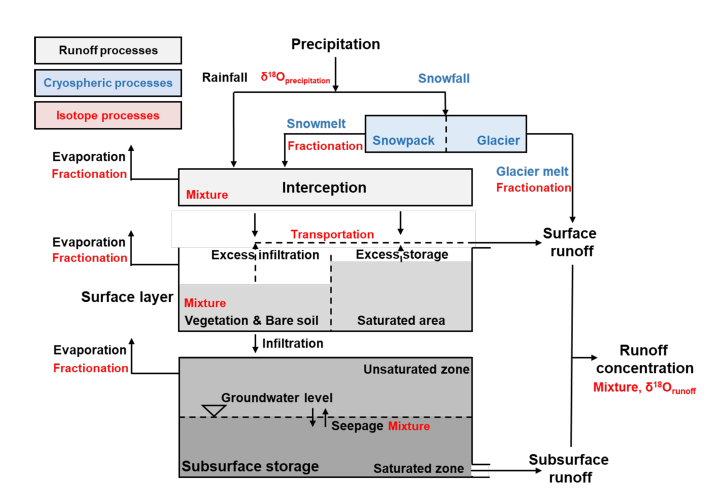


Figure 1. Schematic representation of the THREW-T model

155

160

165

the turnover of snow to ice, and the ice melt. The ice melt was also calculated using the temperature index method but with a different degree-day factor from snowmelt. The volume of the glacier was updated based on the mass balance equation and was transferred to the glacier cover area based on a scale equation (Grinsted (2013))(Grinsted, 2013). The glacier melt was assumed to generate streamflow directly through the surface pathway, considering the low permeability of glacier surface. The output of the glacier simulation included the glacier mass balance (GMB) and the glacier cover area, and the simulated GMB would be compared with the measurement data. More details of the cryospheric module can be found in Nan et al. (2021b) and Cui et al. (2023).

The tracer module was incorporated into the model to simulate the isotope composition in multiple water bodies, which characterized the isotopic variations during water mixture and phase change processes. The isotope fractionation during water evaporation and snowmelt processes was simulated by the Rayleigh equation (Hindshaw et al. (2011)). The glacier meltwater was assumed to have a constant isotope composition, which was more depleted than the average local precipitation isotope by an offset parameter (Nan et al. (2023)). The isotope compositions in each simulation unit were calculated based on the complete mixing assumption, meaning that the tracer concentration homogeneity within a unit was achieved during a simulation time step (Nan et al. (2023)). Forced by the precipitation isotope input, the model can simulate the isotope composition of all the water bodies, including river water, groundwater and snowpack, and the simulated isotope composition of river water would be compared with the observation data. More details of the tracer module are provided in Nan et al. (2021b).

The Contributions of Runoff Components (CRC) were analyzed to better understand the influence of multiple datasets on hydrological simulations. Two definitions are commonly used to quantify CRC (He et al., 2021). One is based on water sources, describing where the water originates; under this definition, the three components are rainfall, snowmelt and glacier melt. The other is based on the runoff generation pathway, describing how water produces runoff; here, the two components are surface and subsurface runoff. The THREW-T model quantified the runoff components based on the definition that combines

water sources and runoff generation pathways(He et al. (2021)). Specifically, the runoff was first divided into surface runoff and subsurface runoff (baseflow) based on the runoff generation pathway. The surface runoff was further divided into three components induced by different water sources: rainfall, snowmelt, and glacier melt. Consequently, the total runoff was divided into four components: subsurface runoff, rainfall surface runoff, snowmelt surface runoff, and glacier melt surface runoff.

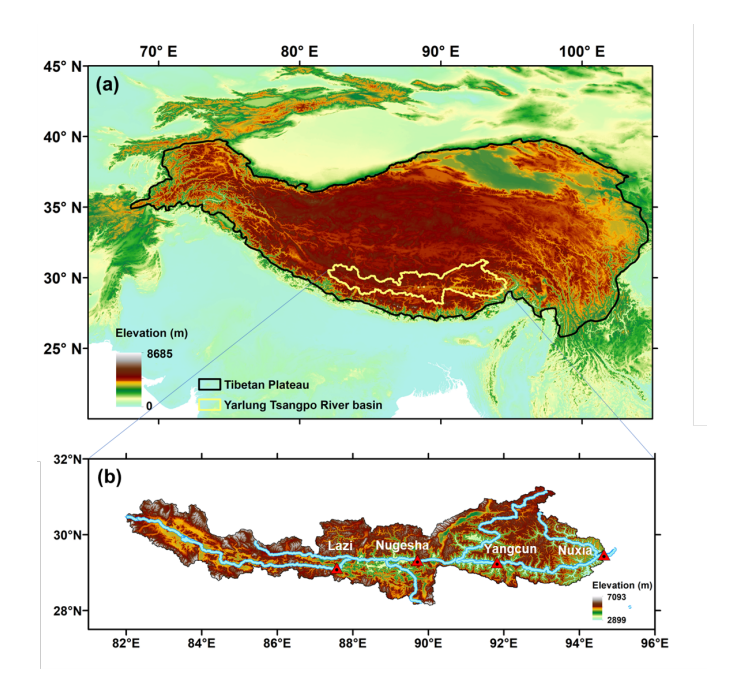


Figure 2. The location and topography of (a) the Tibetan Plateau and (b) the Yarlung Tsangpo River basin

Table 2. Parameter table with descriptions, ranges, and units.

Symbol	Range	Units	Description
nt	0-0.2	_	Manning roughness coefficient for hillslope
WM	0–10	m	Tension water storage capacity used to calculate the sat-
			uration area
В	0–1	_	Shape coefficient used to calculate the saturation area
Gatr	0–10	_	Coefficient representing spatial heterogeneity of ex-
			change term between t-zone and r-zone
KKA	0–6	_	Exponential coefficient to calculate the subsurface
			runoff outflow rate
KKD	0-0.5	_	Linear coefficient to calculate the subsurface runoff out-
			flow rate
DDFs	0–10	mm°C ⁻¹ d ⁻¹	Degree-day factor for snowmelt
$\mathrm{DDF}_{\mathrm{G}}$	0–10	mm°C ⁻¹ d ⁻¹	Degree-day factor for glacier melt
LL	0–1	_	Coefficient to transfer snow water equivalent to snow
			cover area using snow depletion curve
T_0	-5 - 5	°C	Temperature threshold above which snow and glacier
			melting occurs
α	0–1	_	Coefficient in the Muskingum method for runoff con-
			centration calculation
β	0–1	_	The proportion to the α coefficient in the Muskingum
			method for runoff concentration calculation

Parameter table with descriptions, ranges,

and units.

2.3 Multi-objective Parameter Estimation

175

180

195

The uncertainty estimation of model parameters was performed using the Generalized Likelihood Uncertainty Estimation (GLUE) methodology (Beven, 2006). GLUE employs Monte Carlo simulations to generate a large ensemble of model realizations, where each realization corresponds to a specific parameter set associated with a likelihood measure. Unlike traditional optimization methods that focus on identifying a single *best* parameter set, GLUE emphasizes equifinality by retaining an ensemble of acceptable parameterizations (Efstratiadis and Koutsoyiannis, 2010; Brazier et al., 2000), thus acknowledging that multiple parameter sets can produce similarly good simulations, which is particularly important when modeling complex hydrological systems where uncertainties in processes and inputs can lead to varied but equally plausible outcomes (Di Marco et al., 2021).

The selection of likelihood measures and thresholds to distinguish behavioral from non-behavioral simulations is inherently subjective and problem-dependent (Blasone et al., 2008; Jin et al., 2010). In this study, the parameter space was sampled using Latin Hypercube Sampling (LHS) (McKay et al., 1979), assuming a uniform distribution for all parameters listed in Table 1. In the absence of prior information, all parameter sets were initially considered equally probable, ensuring non-informative priors (e.g., Gan et al., 2018; Teweldebrhan et al., 2018). The impact of this uniformity assumption on posterior results was evaluated through sensitivity analyses.

A total of 25,000 parameter sets were generated and evaluated using a likelihood measure to quantify model performance. Behavioral simulations were identified based on a predefined threshold, the value of which is provided in the results section. Non-behavioral simulations were assigned a likelihood of zero, while the likelihood values of retained simulations were rescaled to sum to one, forming a posterior probability density function for the model parameters.

Predictive uncertainty of outputs, such as streamflow, was assessed by ranking behavioral simulations according to their rescaled likelihoods. The empirical cumulative distribution, weighted by these likelihoods, was used to define uncertainty bounds by excluding the lower and upper 5th percentiles (Teweldebrhan et al., 2018; Franks et al., 1998).

The Nash-Sutcliffe Efficiency Index (NSE) (Nash and Sutcliffe, 1970) was selected as the likelihood measure for stream-flow, snow-covered area (SCA), and isotopic composition (I) (Lamontagne and Barber, 2020; Araya et al., 2023), while the Volumetric Deviation Efficiency (VEVE) (He et al., 2018) was adopted for glacier mass balance (GMB). These two metrics were chosen to reflect both dynamic performance and cumulative accuracy across key hydrological variables.

The NSE was used as the likelihood measure for streamflow, snow-covered area, and isotopic composition. Its formulation is provided for completeness:

200
$$\underline{NSE} \underbrace{NSE}_{X} = 1 - \frac{\sum_{t=1}^{N} (X_{sim}(t) - X_{obs}(t))^{2}}{\sum_{t=1}^{N} (X_{obs}(t) - X_{obs,mean})^{2}} \underbrace{\sum_{t=1}^{N} (X_{sim}(t) - X_{obs}(t))^{2}}_{\sum_{t=1}^{N} (X_{obs}(t) - X_{obs,mean})^{2}},$$
(1)

where X represents the variable of interest, $X_{sim}(t)$ and $X_{obs}(t)$ and $X_{obs}(t)$ are the simulated and observed values at time step t, $X_{obs,mean}$ is the mean of the observed values, and N is the number of time steps.

For glacier mass balance (GMB), the Volumetric Deviation Efficiency (VE) was deemed more appropriate as it directly evaluates the accuracy of the simulated mean relative to the observed mean, aligning better with the cumulative nature of GMB:

$$\underline{VE_{GMB}}\underline{VE_{GMB}} = 1 - \frac{GMB_{mean,sim} - GMB_{mean,obs}}{GMB_{mean,obs}} \frac{GMB_{mean,sim} - GMB_{mean,obs}}{GMB_{mean,obs}},$$
(2)

where $GMB_{mean,sim}$ and $GMB_{mean,obs}$ are the simulated and observed mean glacier mass balances, respectively.

The multi-objective parameter estimation followed an informal Bayesian framework. The streamflow likelihood, $LH(Q|p_i)LH(Q|p_i)$.

210 was first used to constrain the model parameters, forming the prior likelihood distribution. Auxiliary variables (X) were then incorporated to produce a posterior likelihood distribution (eLH_{CLH}), defined as:

$$\underline{cLH}\underline{cLH}(p_i|Q,X) = \frac{1}{C} \cdot \underline{LH}\underline{LH}(Q|p_i) \cdot \underline{LH}\underline{LH}(X|p_i), \tag{3}$$

where p_i represents a parameter set, $\frac{LH(Q|p_i)}{LH(Q|p_i)}$ and $\frac{LH(X|p_i)}{LH(Q|p_i)}$ and $\frac{LH(X|p_i)}{LH(Q|p_i)}$ are the likelihoods for streamflow and auxiliary variables, respectively, and C is a normalization constant ensuring:

$$215 \int \underline{cLH} \underline{cLH}(p_i|Q,X) dp_i = 1.$$
(4)

In the absence of explicit guidelines for auxiliary datasets, except for streamflow, a threshold of NSE > 0 and VE > 0NSE > 0 and VE > 0NSE > 0 and VE > 0, commonly used as minimal performance criteria, was systematically applied to all target variables, including streamflow (QQ), snow-covered area (SCA), glacier mass balance (GMB), and isotopic composition (H). The use of NSE > 0 NSE > 0 for streamflow ensures consistency across all metrics, even though stricter thresholds are typically recommended to ensure the reliability of streamflow simulations (Moriasi et al., 2007). Furthermore, following Di Marco et al. (2021); Ma et al. (2024), the 75th percentile was chosen as the cutoff for both the prior and posterior distributions to select parameter sets, ensuring a consistent and robust identification of the most likely parameters while balancing model accuracy and diversity.

2.4 Metrics for Quantifying Uncertainty

220

To assess the added value of multi-objective model conditioning compared to single-objective approaches based solely on streamflow observations, we utilized two uncertainty metrics: the first, known as the containing ratio (CR), evaluates the ability of the simulated prediction intervals to capture the observed values and reads as follows (e.g., Teweldebrhan et al. (2018); Jin et al. (2010)):

$$\underline{CR}\underline{CR} = \frac{1}{\underline{N}} \underbrace{\frac{1}{N}}_{t=1} \sum_{t=1}^{NN} \Gamma \left(Q_{\underline{obs}\underline{obs}}(t); Q_{\underline{sim0.05}\underline{sim,0.05}}(t), Q_{\underline{sim0.95}\underline{sim,0.95}}(t), Q_{\underline{sim0.95}\underline{sim,0.95}}(t) \right), \tag{5}$$

where $Q_{\text{sim}0.05}(t)$ and $Q_{\text{sim}0.95}(t)$ indicate the lower and upper bounds of the simulated 90% streamflow prediction interval, respectively, while Γ returns a value of 1 if the observation falls within the prediction interval and 0 otherwise. A higher

CR value indicates that the prediction intervals are better at capturing observed values, reflecting improved reliability of the model outputs. Conversely, a lower CR suggests that the prediction intervals fail to encompass the observed data as effectively, indicating potential deficiencies in the model's calibration or input data.

The second metric, the so-called sharpness (SH), is a measure that quantifies the reduction in prediction uncertainty achieved through the integration of additional information and reads as follows:

$$\underline{\underline{SH}}\underline{SH} = 1 - \frac{cLH(p_i \mid Q, X)}{LH(Q \mid p_i)} \frac{cLH(p_i \mid Q, X)}{LH(Q \mid p_i)}. \tag{6}$$

A higher SH value signifies that the prediction intervals are narrower, implying reduced uncertainty in the model's predictions and a more precise representation of the streamflow dynamics. On the other hand, a lower SH value suggests broader prediction intervals, indicative of higher uncertainty or less precise modeling.

It is worth noticing that in an ideal scenario, a perfectly constrained model would achieve CR and SH values close to 1. In practice, this would imply that the prediction intervals consistently capture observed values (CR = 1CR = 1) and that the model uncertainty diminishes to the point where the simulated output closely aligns with the observations, indicating that there is no uncertainty in the predictions.

3 Results

250

255

260

245 3.1 Behavioral simulations

For each run of the overall Monte Carlo sample ensemble, we computed likelihood values for streamflow (NSE_O) and additional metrics, including the NSE_O) and for the additional performance metrics: Snow Cover Area likelihood ($NSE_{SCA}NSE_{SCA}$), Glacial Mass Balance likelihood ($\frac{VE_{GMB}}{VE_{GMB}}$), and Isotope likelihood ($\frac{NSE_T}{VE_T}$). The relationships between streamflow likelihood and these additional metrics are presented in Figure bi-objective relationships between NSE_Q and each of these metrics are illustrated in Figure 3, where the Pareto fronts (red markers) represent solutions that optimally balance each panel shows the distribution of the full ensemble of simulations. Specifically, the red markers indicate simulations on the Pareto front, defined as the subset of runs that are non-dominated with respect to the two metrics shown. These points represent optimal trade-offs between conflicting objectives. The dominated solutions(gray points) illustrate the broader solution space , providing insights the objectives, in the sense that no other simulation achieves better performance in one metric without reducing performance in the other. The Pareto front was computed over the entire ensemble and independently of any behavioral classification; red markers should therefore not be interpreted as behavioral simulations. The blue lines in each panel indicate the performance thresholds used to define behavioral solutions, and are included solely as a visual reference. The relatively small number of Pareto-optimal solutions reflects the selective nature of multi-objective trade-offs: only a small subset of parameterizations cannot be outperformed in both objectives simultaneously. This observation is consistent with findings from Di Marco et al. (2021), who showed that Pareto-optimal simulations are typically far fewer than those classified as behavioral. The remaining simulations, shown as gray points, represent dominated solutions, meaning that there exists at least one other

simulation that performs equally well or better across all objectives. These points characterize the broader trade-off space and provide insight into the variability of model performance across different calibration scenarios. The blue lines indicate the minimum performance thresholds for selecting the behavioral solutions the full ensemble.

The Snow Cover Area likelihood (*NSE_{SCA}* NSE_{SCA}) exhibits a strong positive relationship with streamflow likelihood (*NSE_Q* NSE_Q). As shown in Figure 3.a, the Pareto front points (red markers) are concentrated in the upper-right quadrant of the plot, indicating that high streamflow likelihood values can coexist with high *NSE_{SCA}* NSE_{SCA} values. This suggests strong compatibility between these two objectives, meaning that improving streamflow performance does not inherently result in a reduction in *NSE_{SCA}* NSE_{SCA}. The dominated solutions (gray points) show a wider spread across the plot, including regions where both *NSE_Q* and *NSE_{SCA}* NSE_Q and NSE_{SCA} values are low. This indicates variability in model performance when considering different parameter sets. The clustering of Pareto-optimal solutions in the high-likelihood region reflects the shared role of snow processes in regulating both streamflow and snow cover dynamics suggest that it is possible to improve *NSE_{SCA}* NSE_{SCA} without significant trade-offs when calibrating the model to optimize streamflow performance.

The Glacial Mass Balance likelihood ($\overline{VE_{GMB}}\overline{VE_{GMB}}$) shows a slightly different behavior, as illustrated in Figure 3.b. Although high streamflow likelihood values are still associated with moderate to high $\overline{VE_{GMB}}$ VE_{GMB} values on the Pareto front, the vertical spread of the red markers is more pronounced. This indicates a weaker synergy between these two metrics compared to $\overline{NSE_{SCA}}\overline{NSE_{SCA}}$. While some Pareto-optimal solutions achieve high likelihoods for both $\overline{NSE_Q}$ and $\overline{VE_{GMB}}\overline{NSE_Q}$ and $\overline{VE_{GMB}}\overline{NSE_Q}$ and $\overline{VE_{GMB}}\overline{NSE_Q}$ performance. This pattern suggests the presence of moderate trade-offs, where accurately capturing glacial mass dynamics might be compromised to achieve better streamflow performance.

The Isotope likelihood ($NSE_T NSE_I$) exhibits the most significant trade-offs among the three metrics, as illustrated in Figure 3.c. The Pareto front (red markers) is notably dispersed, with even the highest-performing solutions for $NSE_Q NSE_Q$ rarely exceeding an $NSE_T NSE_I$ value of 0.4. This indicates a high degree of independence and conflict between these two metrics. The complexity of this relationship is further emphasized by the dominated solutions (gray points), where many configurations achieve high $NSE_Q NSE_Q$ values but fail to yield satisfactory $NSE_T NSE_I$ values.

3.2 Prior and posterior parameter distributions

265

270

280

285

290

Figure 4 shows the prior (black lines) and posterior distributions for each model parameter parameter distributions, conditioned on snow cover area likelihood (red the likelihoods of Snow-Cover Area (SCA, orange dashed lines), glacier mass balance likelihood (green Glacier Mass Balance (GMB, light blue dash-dotted lines), and isotope data (blue concentrations (I. green dotted lines). A visual inspection of these All distributions are derived from the Monte Carlo ensemble, but only simulations with a Nash–Sutcliffe Efficiency for streamflow ($NSE_Q > 0$) are retained. This threshold ensures that simulations outperform the climatological mean, thereby meeting a minimum criterion for behavioral plausibility. These behaviorally plausible simulations define the prior distribution, which is then formally updated within a Bayesian framework using the likelihoods associated with the additional observational datasets (i.e., SCA, GMB, and I). Visual inspection of the posterior

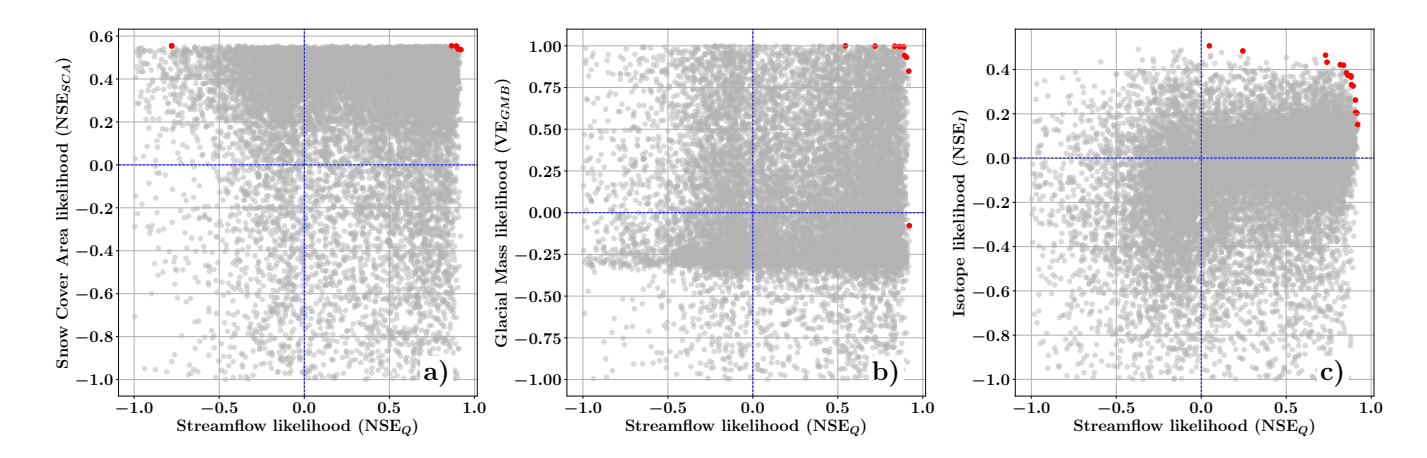


Figure 3. Pareto fronts (red markers) of streamflow likelihood (NSE_QNSE_Q) and likelihood metrics for (a) Snow Cover Area likelihood ($NSE_{SCA}NSE_{SCA}$), (b) Glacial Mass Balance likelihood ($NSE_{GMB}NE_{GMB}$), and (c) Isotope likelihood (NSE_TNSE_I). The thin blue lines represent the performance thresholds defined for the multi-objective behavioral selection: $NSE_Q = 0$, $NSE_{GMB} = 0$, $NSE_{SCA} = 0$, $NSE_{I} = 0$, and $NSE_{GMB} = 0$. The dominated solutions are shown as gray points.

distributions indicates that, in general, each dataset provides meaningful information to constrain parameters specifically linked to the underlying related to the physical processes it represents.

For example, the parameters DDF_S and LL (Figures 4.g and 4.i), which control the snow cover area transfer and snowmelt processes, show a stronger response when conditioned on the likelihood of SCA, highlighting their direct influence on snow dynamics. While DDF_S regulates the magnitude of snowmelt, LL primarily affects the spatial extent and persistence of snow cover. As such, its influence is more pronounced in shaping the spatial and temporal patterns of snow accumulation and melt, rather than the total amount of snowmelt contributing to runoff. This explains why the posterior of LL is well constrained under SCA conditioning, but does not manifest as clearly in metrics focused on water yield, such as snowmelt fraction. Similarly, the parameter DDF_G (Figure 4.h), which governs glacier melt processes, exhibits tighter posterior constraints when conditioned on the GMB likelihood, reflecting its strong connection to ice melt dynamics. Interestingly, the parameter DDF_S shows a contrasting response under the GMB likelihood, with the posterior distribution shifting in the opposite direction compared to the SCA posterior distribution.

300

305

310

A similar observation can be made for the isotopic likelihood, which effectively constrains parameters related to subsurface flow and runoff partitioning. For example, the parameter KKA (Figure 4.e), which defines the subsurface runoff outflow rate, shows noticeable convergence when conditioned on isotope data. Although both KKA and KKD influence subsurface runoff outflow, only KKA shows a marked posterior convergence. This is likely due to its exponential formulation, which increases its sensitivity to the calibration targets, whereas KKD, as a linear coefficient, exerts a more gradual influence that is harder to isolate and constrain. Other parameters, such as the tension water storage capacity WM (Figure 4.b) and the shape coefficient B (Figure 4.c), which influence the calculation of the saturation area, also exhibit tighter posterior distributions, underscoring the capacity of isotope data to inform processes related to water storage and release in the subsurface. Furthermore, the runoff

concentration coefficients α and β (Figures 4.k and 4.l) are better estimated with the inclusion of isotopic data with respect to the likelihoods of SCA and GMB.

An interesting case is the temperature threshold parameter T_0 (Figure 4.j), which defines the threshold above which snow and glacier melting occur. As expected, the Glacier Mass Balance The SCA likelihood has the strongest influence on the posterior distribution of T_0 due to its direct relationship with glacier melt processes. However, both the SCA GMB and the isotopic likelihoods can narrow the posterior distribution of T_0 , albeit to a lesser extent, indicating that the snow cover glacier mass balance and the isotopic data provide complementary constraints on this parameter.

In contrast, the posterior distribution of the parameter Gatr shows minimal variation compared to the previous (Figure 4. d), aligning with expectations, as Gatr reflects spatial heterogeneity, which reduces its sensitivity to individual physical processes. It is also worth noting that for the parameter nt, not only does none of the data sets (SCA, GMB, or I) significantly constrain the posterior distribution compared to the prior, but the isotopic likelihood appears counterproductive in this case, as it increases the uncertainty by broadening the posterior distribution and reducing its peak.

3.3 Streamflow simulation uncertainty range

320

325

330

335

340

345

The prior and posterior likelihood distributions, as described in Section(2) 2, were here used to estimate the 5th–95th percentile prediction uncertainty ranges for daily streamflow simulations. Figure(5) 5 illustrates this predictive uncertainty ranges compared to observed streamflow data recorded at the Nuxia gauging station. The prior predictive uncertainty, represented by dark grey bands, corresponds to the hydrological model conditioned solely on observed streamflow data. In contrast, the posterior uncertainty ranges, depicted by lighter bands, were obtained by integrating additional datasets: snow cover area, glacier mass balance, and isotopic data.

The uncertainty bands proved to be overall effective in capturing observed streamflow values. Specifically, the containing ratio (CR) metric indicates that the prior distribution encloses approximately 96% of the observed streamflow values (CR = 0.959). Posterior distributions derived from isotopic likelihoods exhibit a slightly reduced CR of 0.921, while those based on SCA and GMB yield CR values of 0.947 and 0.960, respectively. These findings suggest that, while SCA and GMB maintain similar levels of coverage compared to the prior, they do not lead to a substantial reduction in predictive reliability. Conversely, the posterior conditioned on isotopic data demonstrates a modest decrease in coverage.

Visual inspection of Figure(5) 5 indicates no reductions in uncertainty bands for higher streamflow values across all scenarios. On the contrary, the most pronounced contraction of predictive uncertainty occurs during low-flow periods when the model is conditioned with isotopic data (Figure 5.e), whereas conditioning with SCA and GMB does not produce comparable reductions, Figures(5.a) and (and 5.c) respectively. Besides, Flow Duration Curves (FDCs), presented in the right panels of Figure(5) 5, provide further insights into the impact of these datasets across different flow regimes. For SCA and GMB (FigureFigure 5.b and 5.d), the posterior uncertainty ranges are generally comparable to or slightly narrower than the prior for medium-flow regimes. During low-flow conditions, however, the posterior bands are wider than the prior, indicating that incorporating SCA and GMB datasets introduces additional variability in streamflow predictions during baseflow-dominated low flow dominated periods, likely due to challenges in accurately constraining slow-response hydrological processes. For medium-flow dominated periods, likely due to challenges in accurately constraining slow-response hydrological processes.

and high-flow regimes, these datasets appear to modestly refine or maintain predictive uncertainty. In contrast, conditioning the model with isotopic data (Figure 5.f) results in a significant reduction in uncertainty, particularly during low-flow conditions. In contrast, conditioning the model with isotopic data (Figure 5.f) results in a significant reduction in uncertainty, particularly during low-flow conditions. The posterior uncertainty range is substantially narrower than the prior, suggesting that isotopic data provide robust constraints on processes governing baseflow and subsurface contributions. indicating improved model consistency in simulating low flow dominated periods.

These patterns of uncertainty reduction—particularly the distinct effect of isotopic data during low-flow periods—are also evident at the Yangcun and Nugesha stations (Figures S6 and S7 in the Supplementary Material), further supporting the conclusions presented above.

3.4 Runoff component analysis

350

355

360

365

370

375

380

Figure 6 shows the CRC produced by different behavioral parameter sets. The boxplots illustrate the contributions of the four runoff components under the prior parameter set and the posterior parameter sets constrained by snow cover area, glacier mass balance, and isotope likelihoods. The contributions of subsurface runoff and rainfall surface runoff are similar, both accounting for approximately 40–45% of the total runoff (Figure 6.a and 6.b). In contrast, snowmelt surface runoff and glacier melt surface runoff contribute approximately 8% and 6%, respectively (Figure 6.c and 6.d). The estimated contributions of snowmelt and glacier melt are lower than some previous estimations in the study area (Boral and Sen, 2020; Lutz et al., 2014), but are close to some recent studies constraining the CRC estimation based on multiple datasets (Nan et al., 2025; Zhang et al., 2025; Chen et al., 2017)

The differences in the average CRCs among the parameter sets are relatively small, with variations generally below 3% for all four components. However, the inferences drawn from the different datasets reveal interesting patterns regarding uncertainty reduction. The prior leads to a wider distribution of contributions across all runoff components, reflecting higher uncertainty in the model predictions. Posterior parameter sets constrained by specific datasets help reduce this uncertainty to varying extents. Constraining the model with the likelihood of glacier mass balance leads to a significant reduction in the uncertainty of glacier melt surface runoff (Figure 6.d), as evidenced by the tighter interquartile range and fewer outliers in the box plot. This indicates that the GMB simulation provides strong constraints on glacier-related processes. In contrast, the snow cover area does not lead to a significant reduction in the uncertainty of snowmelt surface runoff (Figure 6.c). This is because SCA data only constrains the area of snow but does not provide much constraint on the volume of snow, as the snow area-volume relation is determined by a calibrated parameter. Notably, the isotope likelihood demonstrates a broader impact on reducing uncertainty across multiple runoff components. The boxplots for £1 show narrower distributions for subsurface runoff, rainfall surface runoff, and snowmelt surface runoff, indicating that isotope simulation provides valuable constraints on both surface and subsurface hydrological processes.

The influence of each dataset on CRC uncertainties can be further illustrated by the result of sensitivity analysis, which evaluates the extent to which each performance metric to is influenced by the contribution of each runoff component. To this end, Figure 7 presents the sensitivity of model performance metrics to the contributions of different runoff components,

namely subsurface runoff ($C_{ss}C_{ss}$), rainfall surface runoff ($C_{sr}C_{sr}$), snowmelt surface runoff ($C_{sm}C_{sm}$), and glacier melt surface runoff ($C_{sgm}C_{sgm}$). The sensitivity analysis evaluates the extent to which each performance metric—streamflow NSE(Q) metric—streamflow NSE_Q , snow cover area NSE(SCA) NSE_{SCA} , glacier mass balance VE(GMB) VE_{GMB} , and isotope NSE_{I} —is influenced by the relative contribution of each runoff component to total streamflow.

385

390

395

400

The results indicate that streamflow performance NSE(Q) NSE_Q and snow cover area performance NSE(SCA) NSE_{SCA} respond differently to variations in the contribution of individual runoff components. While $\frac{NSE(SCA)}{NSE_{SCA}}$ remains largely insensitive to CRC variations, showing consistently high values across a wide range of runoff component contributions, NSE(Q)-NSE_Q exhibits a more noticeable response. The scatterplots reveal that although streamflow performance remains relatively high ($\frac{NSE}{>}0.8$ NSE_Q > 0.8) even when CRC deviates from its optimal value, there is a clear tendency for behavioral solutions to cluster towards an optimal CRC, indicating a degree of sensitivity. In contrast, glacier mass balance performance VE(GMB) VE_{GMB} shows strong sensitivity to glacier melt runoff C_{sam} , with VE(GMB) C_{sgm} , with VE_{GMB} dropping significantly when C_{sgm} exceeds approximately 10%. The most pronounced sensitivity is observed in the isotope performance metric $NSE(I)NSE_I$, which responds to variations in multiple runoff components. The scatterplots reveal that NSE(I)- NSE_I declines markedly when the contributions of subsurface runoff C_{ss} C_{ss} , rainfall runoff C_{sr} C_{sr} , or snowmelt runoff C_{sm} deviate from optimal values. In particular, $\frac{NSE(I)}{NSE_I}$ decreases significantly from 0.4 to below 0.2 when the contributions of these components shift, indicating that isotopic simulations are much more sensitive to changes in runoff contributions compared to other performance metrics. This sensitivity underscores the importance of accurately quantifying the partitioning of different runoff components to achieve reliable isotope-based model predictions. Overall, the analysis highlights that $\frac{VE(GMB)}{VE_{GMB}}$ simulations are primarily sensitive to glacier melt runoff, whereas isotope-based simulations $\overline{NSE(I)}$ NSE_I are more sensitive to a broader range of runoff components.

It is worth noting that, although NSE is not ideally suited to capture spatial features of snow cover dynamics, our analysis focuses on the catchment-integrated snow-covered area, for which NSE remains an informative metric to evaluate the agreement between observed and simulated temporal patterns of areal extent. In this regard, to better assess model performance, we provide the time series of observed versus simulated SCA in Figure S3, along with corresponding comparisons for glacier mass balance and isotopic signatures in Figures S4 and S5 of the Supplementary Material. These visualizations allow the reader to evaluate the temporal evolution and potential systematic biases for each variable, together with the associated posterior predictive uncertainty ranges for SCA, GMB, and isotopic data.

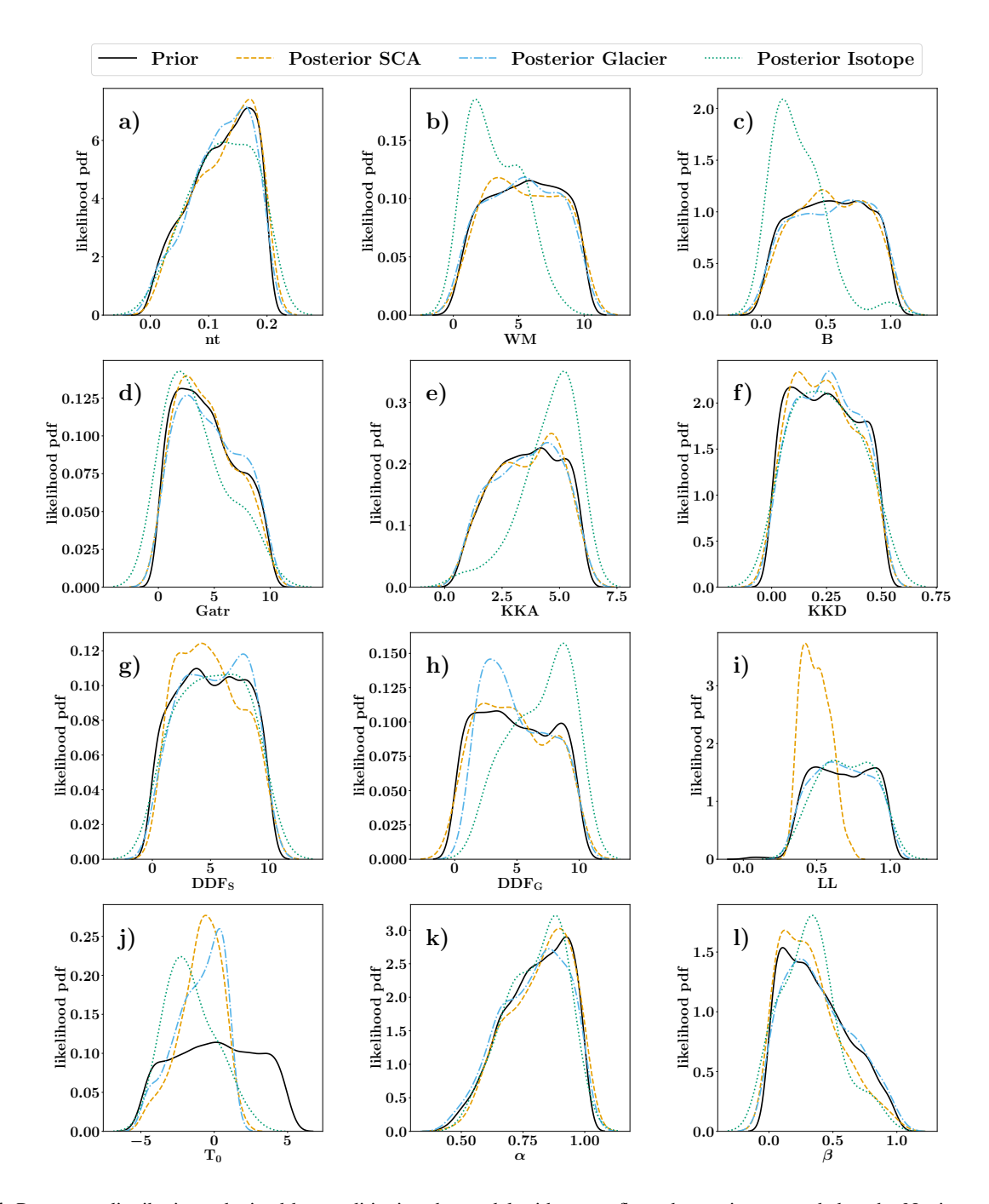


Figure 4. Parameter distributions obtained by conditioning the model with streamflow observations recorded at the Nuxia station (prior pdfPDF, black lineline) and by combining streamflow measures with: (i) eovered snow cover area (posterior pdfPDF, blue orange dashed line); (ii) glacier mass balance (posterior pdfPDF, green light blue dash-dotted line); and (iii) isotope concentration concentrations (posterior pdfPDF, red-green dotted line).

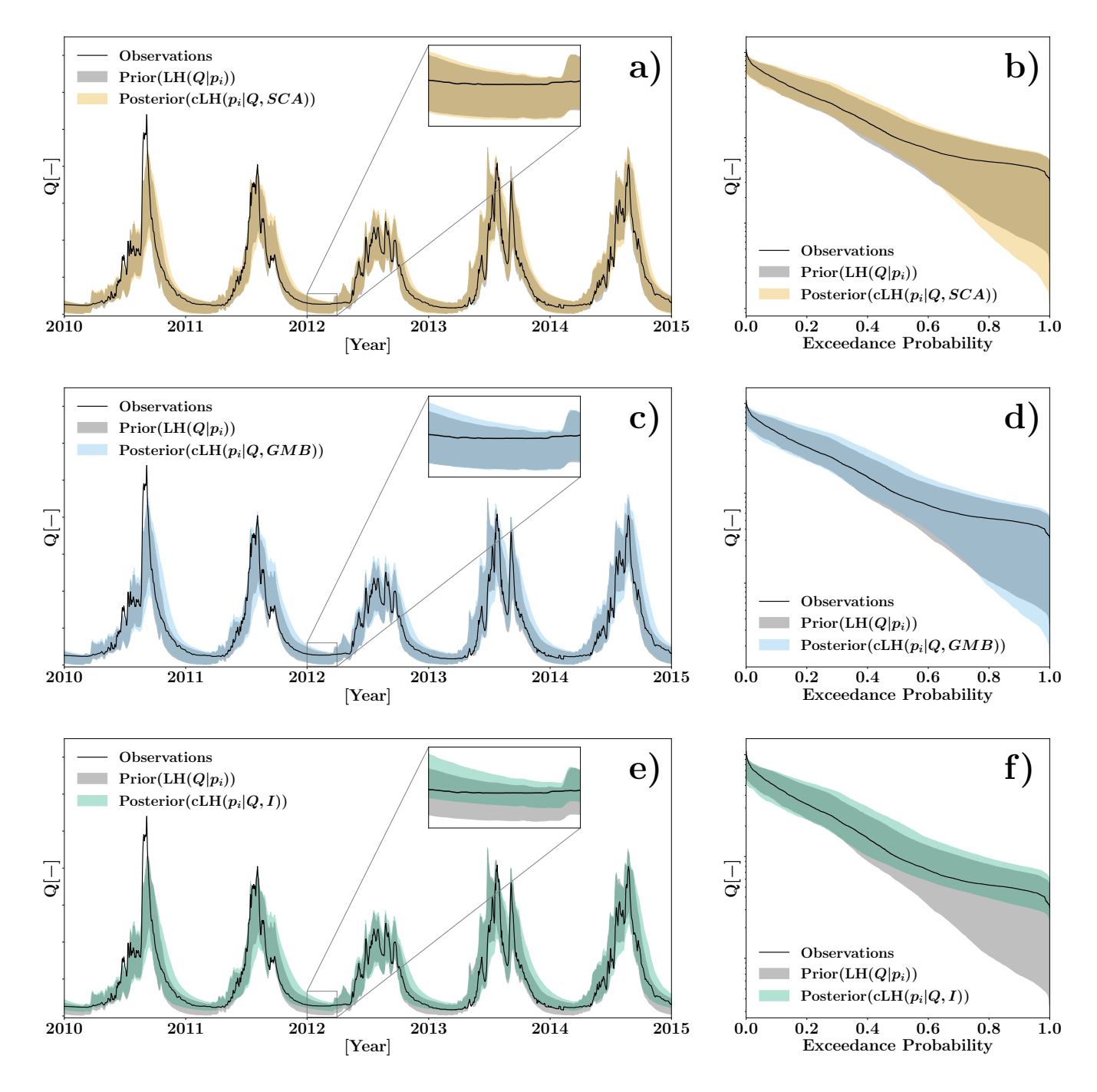


Figure 5. The 5–95% percentile prior, conditioned solely on streamflow, and posterior predictive uncertainty ranges for streamflow, calculated under different conditions: snow cover area (SCA), glacier mass balance (GMB), and isotopes (I). Left panels: daily streamflow time series for the period 2010–20152010-2015, with insets showing zoomed views of low-flow dynamics; right panels: flow duration curves for the entire period 2001–2015. Streamflow data are presented in dimensionless form due to dissemination restrictions imposed by the data provider.

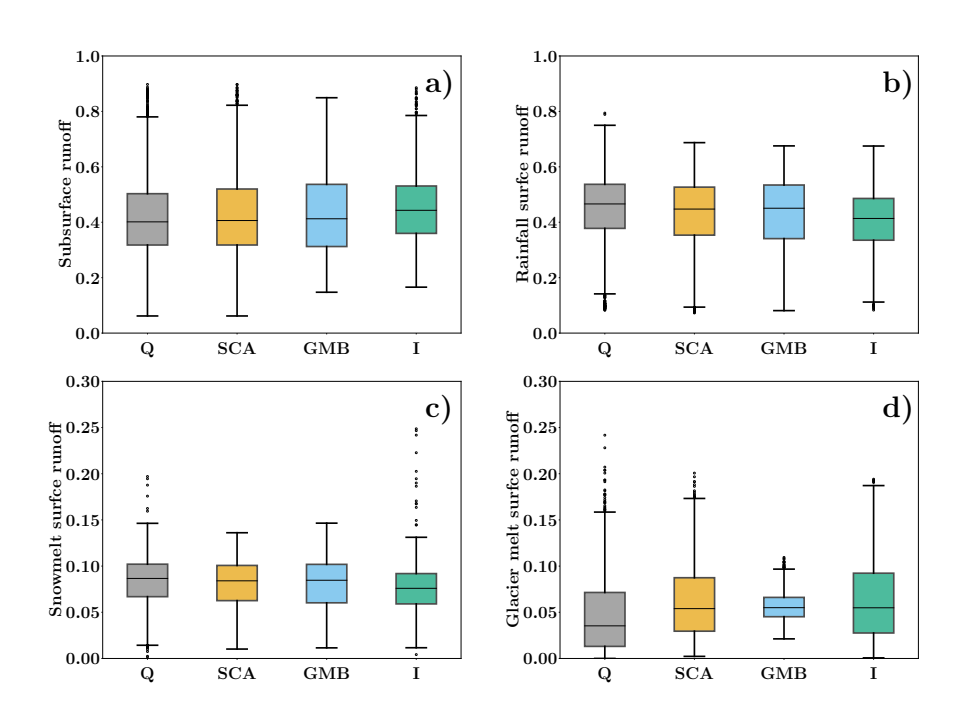


Figure 6. Boxplots showing the variability in the contributions of different surface runoff components under prior estimates conditioned solely on streamflow (Q) and posterior estimates conditioned on additional datasets: snow cover area (SCA), glacier mass balance (GMB), and isotopic data (I). Panel (a): Subsurface runoff; panel (b): rainfall surface runoff; panel (c): Snowmelt surface runoff; panel (d): glacier melt runoff.

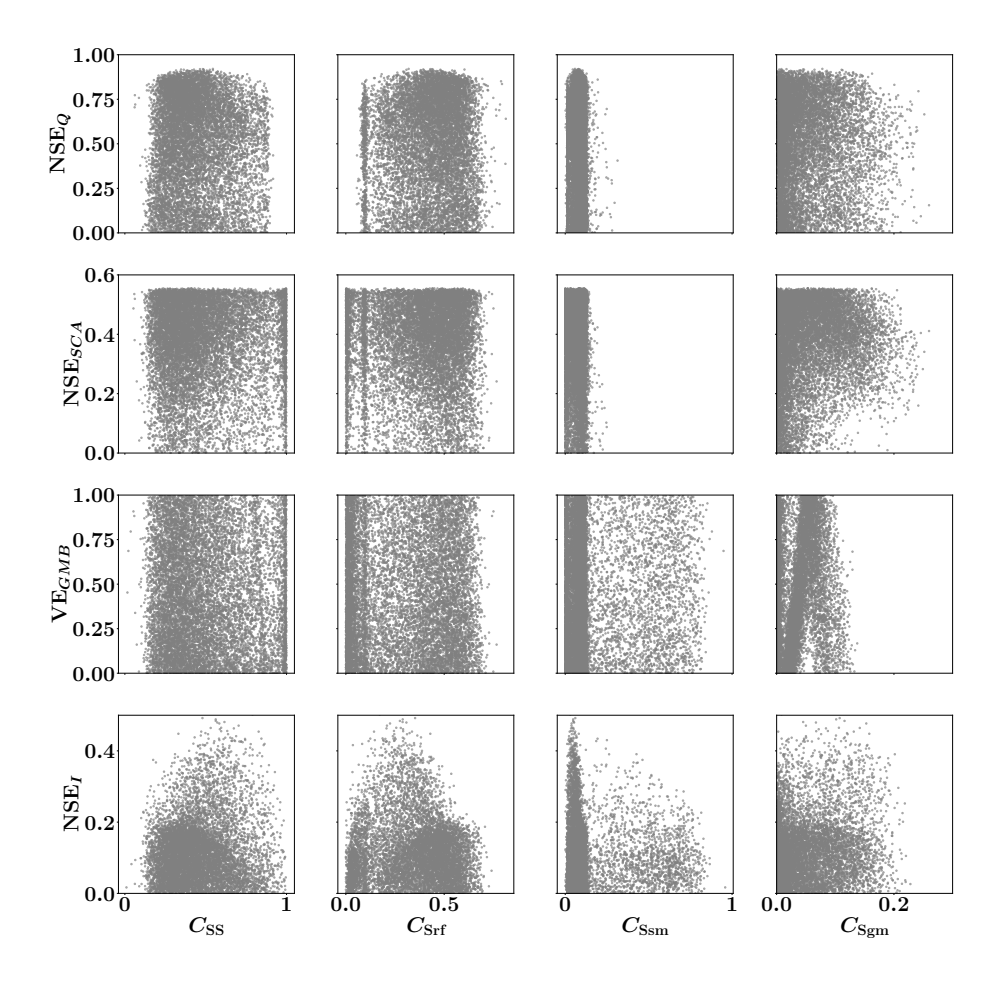


Figure 7. Sensitivity of model performance metrics to runoff component contributions: streamflow $NSE_{CN}NSE_{Q}$, snow cover area $NSE_{SCA}NSE_{SCA}$, glacier mass balance $VE_{GMB}VE_{GMB}$, and isotopes $NSE_{T}NSE_{L}$, plotted against subsurface runoff ($C_{SS}C_{SS}$), rainfall surface runoff ($C_{ST}C_{SL}$), snowmelt surface runoff ($C_{ST}C_{SL}$), and glacier melt surface runoff ($C_{ST}C_{SL}$). Each point represents a behavioral solution from the multi-objective calibration.

410 4 Discussion

415

420

425

430

435

440

Overall, the results presented in Section 3 highlight the differential value of auxiliary datasets in hydrological model calibration. While SCA and GMB provide insights into snow and glacier dynamics, they appear less effective in reducing streamflow uncertainty. Not only do the results prove that integrating multiple data sources within the Bayesian framework influences both streamflow simulation uncertainties and the computation of CRC components, but they also show varying effects depending on the type of dataset and runoff component considered, as discussed below.

4.1 Reducing Streamflow Model Uncertainty Using a Bayesian framework

The results of this study differ in another perspective from those of Di Marco et al. (2021), who observed a consistent relationship in snow-dominated basins between an increased likelihood of streamflow and snow cover area (SCA), alongside a reduction in streamflow uncertainty. In contrast, our findings do not show a comparable narrowing of streamflow uncertainty bands when applying the Bayesian filtering approach with snow and glacier parameters (Figure 5). This discrepancy suggests that the coupling between snow and glacier dynamics and streamflow performance is not straightforward, particularly in larger or more heterogeneous catchments.

As noted by Ruelland (2024), the potential for snow data to enhance streamflow simulation consistency and robustness depends on various factors, including hydro-climatic conditions, spatial variability, the modeling framework, and the accuracy of snow cover data (Hao et al., 2022) and input forcing (Raleigh et al., 2015). Factors such as catchment complexity, spatial heterogeneity, and structural uncertainties in the model—stemming from unresolved hydrological processes or oversimplified dynamics—likely contribute to the persistence of wide uncertainty ranges. In contrast, isotopic likelihoods effectively constrain the parameter space, resulting in improved simulation performance and reduced uncertainty bands, particularly during low-flow conditions. This finding confirms the ability of isotopic data to capture key hydrological processes, such as groundwater-surface water mixing and subsurface flow dynamics, which are especially influential during low-flow periods (Jasechko and Taylor, 2015), where seasonality plays a critical role (Bierkens et al., 2001; Birkel et al., 2009).

The influence of hydrological processes seasonality on the effectiveness of likelihoods is demonstrated by the sharpness polar plot (Figure 8). This figure illustrates the sharpness ranges for posterior likelihoods conditioned on SCA, GMB, and I datasets throughout the year. A maximum SH value of 0.34 was observed for isotopes on March 16, 2008, while the maximum SH values for SCA and GMB were 0.19 on April 30, 2009, and 0.16 on June 10, 2009, respectively. These results highlight the effectiveness of isotopic likelihoods during winter and early spring, with sharpness values remaining consistently narrow and never dropping below zero, when baseflow and subsurface hydrological processes dominatea period when the model indicates a predominance of contributions from the subsurface flow component. In contrast, SCA and GMB likelihoods achieve their sharpness peaks during spring and early summer, coinciding with periods of rapid snowmelt and glacier runoff. This pattern underscores the importance of integrating SCA and GMB likelihoods for capturing high-flow dynamics and highlights the need to further develop these datasets to enhance their effectiveness in constraining streamflow uncertainty during these critical periods.

The results underscore the strengths and limitations of the Bayesian approach in capturing both rapid surface dynamics At this point, it is important to recall that sharpness refers to the degree of concentration of the ensemble simulations where a sharper ensemble has a narrower spread, indicating higher predictive confidence (Gneiting et al., 2007). However, increased sharpness does not necessarily translate into improved reliability. In our case, the inclusion of isotopic data led to a more constrained ensemble, resulting in a sharper posterior distribution of streamflow simulations. While this outcome reflects the stronger constraining power of isotopic information, it also increased the likelihood that observed values fall outside the model's predictive bounds, thereby reducing the containing ratio (CR). Compared to calibrations using snow-covered area (SCA) or glacier mass balance (GMB), the sharper ensemble derived from isotope-informed calibration was less able to fully capture observed variability. This illustrates the classic trade-off between predictive confidence and reliability — in other words, between sharpness and containing ration — in probabilistic modeling (Beven and Binley, 1992), and emphasizes the need to balance these aspects when evaluating ensemble-based hydrological simulations.

These results confirm that isotopic data are highly effective in reducing model uncertainty by providing independent constraints on flow partitioning and subsurface processes. However, to translate this enhanced internal consistency into improved predictive coverage, future research should explore model structural refinements that better align sharpness with CR. Furthermore, these findings illustrate both the potential and the limitations of Bayesian inference in simultaneously capturing fast surface runoff and slower subsurface processes. While the sharpness values reflect its ability dynamics. Although sharpness values demonstrate its capacity to constrain parameter uncertainty across different diverse hydrological processes, alternative approachescalibration strategies, such as multi-objective weighted ealibration, may further enhance optimization, may offer additional improvements in streamflow simulation accuracy (He et al., 2019). HoweverStill, the sensitivity of model accuracy and uncertainty analysis outputs to weight selection necessitates careful consideration during implementation (Tong et al., 2021, 2022). Finally, the interplay between the likelihoods highlights likelihood functions underscores the metric-dependent nature of parameter uncertainty reduction , underscoring the importance and the value of integrating multiple metrics for robust calibration, owing to the strong dependence of calibration outcomes on the evaluation metric adopted complementary evaluation criteria during calibration (e.g., Fenicia et al., 2018; Majone et al., 2022).

These results also point to the need for improved coupling and integration of individual model components. Such integration would allow for better exploitation of the strengths of each dataset and enhance the Bayesian framework's capability to constrain parameter ranges across diverse hydrological conditions. By addressing these structural connections and leveraging synergies between complementary metrics, the Bayesian framework's potential to optimize parameter calibration and improve predictive accuracy can be fully realized.

4.2 Runoff Component Uncertainty

445

450

455

460

470

475

The GMB dataset effectively reduces uncertainty in glacier melt surface runoff simulations (Figure 6.d), emphasizing its value for improving model constraints in glacier-dominated systems. This finding aligns with previous studies highlighting the importance of incorporating GMB data to enhance streamflow predictions in such catchments (Stahl et al., 2008; O'Neel et al., 2014; Yang et al., 2024). However, this reduction in uncertainty does not always translate into improved streamflow

predictions at the basin scale. The effectiveness of the Bayesian framework in reducing uncertainties depends on the proportion of runoff attributed to glacier melt processes. Consequently, even when glacier-related dynamics are well constrained by GMB data, their contribution to reducing overall streamflow prediction uncertainty may be limited in basins where other processes dominate. This underscores the importance of considering basin scale and dominant runoff processes when selecting datasets for hydrological modeling.

Similarly, SCA datasets provide valuable constraints on snowmelt surface runoff (Figure 6.c) but have a more limited impact on reducing streamflow uncertainty. This may be due to the spatial and temporal resolution limitations of SCA datasets (Di Marco et al., 2020), or because the snowmelt contribution to total runoff is relatively minor in large basins compared to other components, such as subsurface runoff and rainfall surface runoff. Furthermore, uncertainties in the timing and rate of snowmelt, which are critical for runoff generation, may not be fully captured by remotely sensed SCA data (Andreas Juergen Dietz and Dech, 2012). This limitation is particularly relevant in basins with complex snow dynamics, where snow cover depletion varies significantly across different elevation bands and time periods (Molotch and Margulis, 2008).

In contrast, isotopic data stand out for their ability to reduce uncertainty across multiple runoff components, particularly during low-flow conditions. By tracing water sources and pathways, isotopic tracers provide critical insights into subsurface and groundwater contributions, which are difficult to capture with traditional datasets (Birkel et al., 2015). Isotopic tracers, such as oxygen-18 (δ^{18} O) and deuterium (D), are widely used to distinguish between recent precipitation, snowmelt, and groundwater contributions to streamflow, improving the calibration of hydrological models (Jasechko, 2019). Our results show that the isotope data does not reduce the uncertainty of glacier melt runoff, because the model assumes that glacier melt generate runoff directly through surface pathway, not involved in the surface-subsurface runoff partitioning, the aspect for which isotopic data are most useful. The results suggest that incorporating isotopic data into hydrological models can help reduce uncertainties related to water source contributions and flow pathways, particularly in catchments with complex surface-subsurface interactions. Such benefit comes from the significant divergence in the isotope signatures of surface and subsurface runoff, i.e., a much lower temporal variability of groundwater isotope compared to surface runoff because of the long travel time.

These differences in the influence of datasets underscore the importance of selecting appropriate data sources based on the specific hydrological processes and uncertainties that need to be addressed in a given catchment. For example, GMB data should be prioritized in glacier-fed basins to improve predictions of glacier melt runoff (Huss and Hock, 2015), whereas isotope data can provide valuable constraints on multiple runoff components, particularly in catchments with diverse flow generation processes (Rodgers et al., 2005; Birkel et al., 2011). The integration of multi-source datasets can help reduce model uncertainties more effectively than relying on a single dataset (Beven, 2006), resulting in more robust predictions of water availability and streamflow variability under changing climatic conditions (Borriero et al., 2023).

4.3 Limitations

480

485

490

495

500

505

510

This study systematically evaluates the value of snow cover area, glacier mass balance, and isotopes in reducing model uncertainties. Results highlight the critical role of isotope data in improving low-flow simulations and runoff component separation.

However, several limitations persist. First, while streamflow simulations achieve NSE values up to 0.9, peak flows are consistently underestimated, likely due to inaccuracies in precipitation forcing data (Jiang et al., 2022; Xu et al., 2017). Metrics for SCA and isotope simulations remain around 0.5, indicating potential for further optimization. Second, the model structure is rather simplified when conceptualizing processes such as groundwater and snow/ice melting. In specify, only two subsurface layers (u-zone and s-zone in the model) are defined, and the subsurface outflows are simulated as a sum. Only the shallow groundwater processes are considered, only occurring within each REW, which is unable to adequately describe subsurface processes in the TP, where deep interbasin groundwater pathways exist (Chen et al., 2025). Meanwhile, the simple degree-day factor method was used to simulate the melting processes, to make the model adequately efficient for subsequent GLUE analysis. These modules can be improved to strengthen the physical basis of the model. Third, as this analysis is based on a single case study in a specific region, its broader applicability is uncertain. Unlike prior studies (Di Marco et al., 2021; Tong et al., 2021), snow and glacier datasets did not significantly enhance model performance here, suggesting the need to clarify the conditions under which such data prove most beneficial.

Despite these challenges, the study underscores the importance of employing multiple datasets to constrain hydrological models. Although snow and glacier datasets alone may not substantially improve streamflow simulations, they are essential for ensuring model reliability in capturing key processes. Isotope data, in particular, effectively constrain surface and subsurface runoff separation due to the low variability in groundwater isotopic composition (Nan et al., 2024; McGuire and McDonnell, 2006), reducing baseflow low flow uncertainties and enhancing model robustness.

5 Conclusions

515

520

525

530

535

540

This study provides new insights into reducing uncertainty and equifinality in the hydrological modeling of large mountainous catchments by integrating multiple auxiliary datasets within a Bayesian framework. By systematically comparing the contributions of snow cover area (SCA), glacier mass balance (GMB), and isotopic tracers, we demonstrate how these datasets distinctly improve model performance across various flow regimes.

A critical conclusion drawn from this research is the unique advantage of isotopic data in reducing model uncertainty during low-flow periods. The isotopic likelihood has shown to be more effective in constraining baseflow-subsurface flow contributions and groundwater-surface water interactions, resulting in narrower uncertainty ranges for streamflow predictions under low-flow conditions. This finding underscores the critical role of isotopic tracers in improving the representation of slow-response hydrological processes, which are essential for the mitigation of drought and sustainable management of water resources in mountainous regions. In contrast, the SCA and GMB datasets were found to be more effective in capturing rapid surface dynamics, such as snowmelt and glacier melt processes. However, their contributions to reducing streamflow uncertainty were limited, particularly during low-flow conditions. This discrepancy highlights the need for multi-objective calibration approaches that balance the trade-offs between rapid surface responses and slow subsurface processes.

Our results also reveal the differential impact of each dataset on the contributions of runoff components. The glacier mass balance likelihood significantly reduces uncertainty in glacier melt surface runoff, whereas isotopic data provide broader con-

straints across multiple runoff components, including subsurface runoff, rainfall surface runoff, and snowmelt surface runoff.

These differences emphasize the importance of selecting appropriate datasets based on the dominant hydrological processes in a given catchment.

The study further highlights the limitations of current Bayesian frameworks in fully leveraging the complementary strengths of auxiliary datasets. While Bayesian approaches are effective in reducing parameter uncertainty and improving model calibration, the persistent wide uncertainty ranges for streamflow predictions indicate the need for improved coupling and integration of individual model components. Enhancing these structural connections within the modeling framework could allow for better exploitation of multi-source datasets, ultimately improving predictive accuracy across diverse hydrological conditions.

550

555

In conclusion, our findings stress the importance of incorporating multi-source datasets in hydrological modeling to achieve robust performance across different flow regimes. The integration of isotopic tracers, snow cover, and glacier mass balance data within a Bayesian framework offers a promising pathway to reduce uncertainty and enhance the understanding of streamflow variability in large mountainous catchments. Future research should focus on developing more advanced coupling methods that account for the complex interplay between cryospheric and subsurface processes, as well as exploring the potential of multi-objective weighted calibration approaches to further improve model reliability.

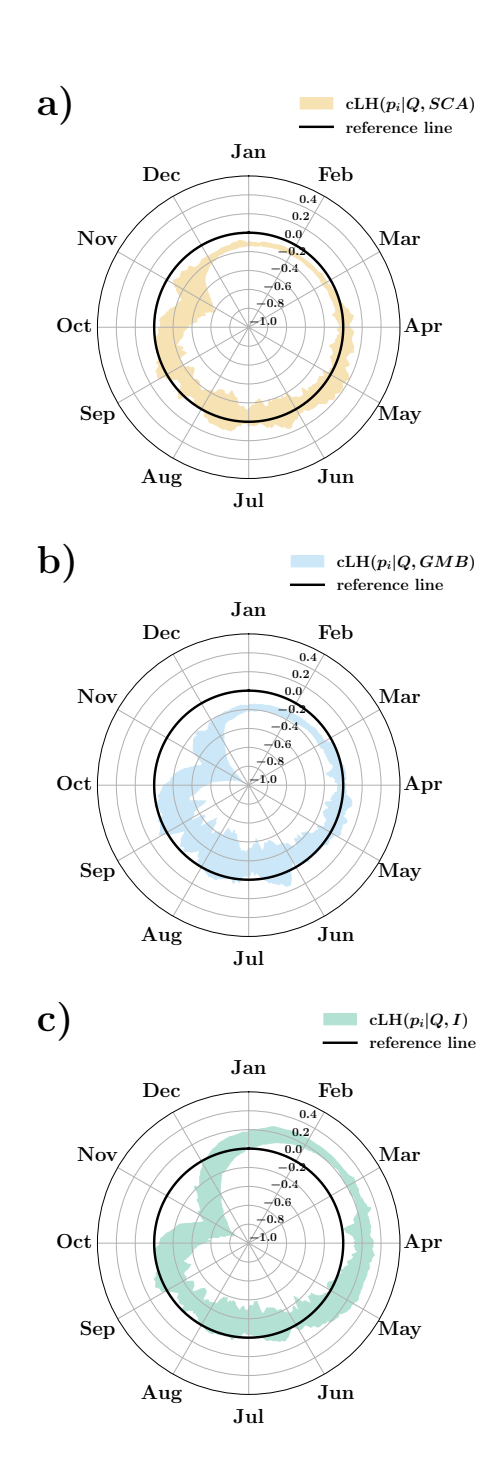


Figure 8. Polar plots showing the daily sharpness band computed from the maximum and minimum sharpness values across the years 2010–2015. The shaded regions represent the range of sharpness variability for each day of the year, while the solid black line indicates the reference level at zero sharpness. The subplots illustrate the sharpness calculated under different conditioning: $eLH(p_i|Q,SCA)$ cLH($p_i|Q,SCA$) (a), $eLH(p_i|Q,GMB)$ (b), and $eLH(p_i|Q,I)$ cLH($p_i|Q,I$) (c).

Code availability

The code of THREW-T model used in this study are available from the corresponding author (ny1209@qq.com).

560 Data availability

Code availability. The code of THREW-T model used in this study are available from the corresponding author (ny1209@qq.com)

Data sets are publicly available as follows: DEM (http://www.gscloud.cn/sources/details/310?pid=302, last access: 1 January 2019, Geospatial Data Cloud Site, 2019), CMFD (https://doi.org/10.11888/AtmosphericPhysics.tpe.249369.file, Yang and He, 2019), glacier inventory data (https://doi.org/10.3972/glacier.001.2013.db, Liu, 2012), glacier elevation change data (https://doi.org/10.6096 Huggonet et al., 2021), NDVI (https://doi.org/10.5067/MODIS/MOD13A3.006, Didan, 2015), LAI (https://doi.org/10.5067/MODIS/MOD Myneni et al., 2015), HWSD (https://doi.org/10.5067/hans/data/3519536a-d1e7-4ba1-8481-6a0b56637baf/?q=HWSD, last access: 1 January 2019, He, 2019). These datasets not publicly available are referred to in the main text (Chen et al., 2018; Liu et al., 2007)

Data availability. Data sets are publicly available as follows: DEM (http://www.gscloud.cn/sources/details/310?pid=302, last access: 1 Jan100 uary 2019, Geospatial Data Cloud Site, 2019), CMFD (https://doi.org/10.11888/AtmosphericPhysics.tpe.249369.file, Yang and He, 2019),
101 glacier inventory data (https://doi.org/10.3972/glacier.001.2013.db, Liu, 2012), glacier elevation change data (https://doi.org/10.6096/13,
101 Huggonet et al., 2021), NDVI (https://doi.org/10.5067/MODIS/MODIS/MODI3A3.006, Didan, 2015), LAI (https://doi.org/10.5067/MODIS/MODI5A2H.006,
102 Myneni et al., 2015), HWSD (https://data.tpdc.ac.cn/zh-hans/data/3519536a-d1e7-4ba1-8481-6a0b56637baf/?q=HWSD, last access: 1 January 2019, He, 2019). The simulated streamflow, snow cover area, glacier mass balance and isotope data produced by the behavioral parameters are available at Zenodo (doi: 10.5281/zenodo.15605202). These datasets not publicly available are referred to in the main text (Chen et al., 2018; Liu et al., 2007

Competing interests

At least one of the (co-)authors is a member of the editorial board of Hydrology and Earth System Sciences.

580 Competing interests. At least one of the (co-)authors is a member of the editorial board of Hydrology and Earth System Sciences.

Acknowledgements. During the preparation of this work the author(s) used ChatGPT in order to improve language and readability of the original draft, with caution. After using these tools, the author(s) reviewed and edited the content as needed and take(s) full responsibility for the content of the publication This study has been supported by the National Natural Science Foundation of China (grant no. 52309023) and the Fund Program of State Key Laboratory of Hydroscience and Engineering (sklhseTD-2024-C01). Diego Avesani acknowledges the Italian Ministry of Education, Universities and Research (MUR), in the framework of the project DICAM-EXC [Departments of Excellence 2023–2027, grant L232/2016]; and the support from the European Union – FSE-REACT-EU, PON Research and Innovation 2014–2020 DM1062/2021; PAT Project Drought Indicators - CUP C97G22000460003. The open-access publication of this study is supported by the Fund Program of State Key Laboratory of Hydroscience and Engineering (sklhseTD-2024-C01).

585

Author contributions. DA was responsible for conceiving the study; developing the methodology; acquiring funding; carrying out the investigation; developing the software; preparing, reviewing, and editing the manuscript; and supervising the study. YN conceived the study, contributed to developing the software, carrying out the investigation, creating the figures, curating the data, and reviewing and editing the manuscript; FT reviewed and edited the manuscript, and supervised the study.

References

600

- Andraos, C.: Breaking Uncertainty Barriers: Approximate Bayesian Computation Advances in Rainfall–Runoff Modeling, Water, 16, 595 https://doi.org/10.3390/w16233499, 2024.
 - Andreas Juergen Dietz, Claudia Kuenzer, U. G. and Dech, S.: Remote sensing of snow a review of available methods, International Journal of Remote Sensing, 33, 4094–4134, https://doi.org/10.1080/01431161.2011.640964, 2012.
 - Araya, D., Mendoza, P., Muñoz-Castro, E., and Mcphee, J.: Towards robust seasonal streamflow forecasts in mountainous catchments: impact of calibration metric selection in hydrological modeling, Hydrology and Earth System Sciences, 27, 4385–4408, https://doi.org/10.5194/hess-27-4385-2023, 2023.
 - Asong, Z. E., Elshamy, M. E., Princz, D., Wheater, H. S., Pomeroy, J. W., Pietroniro, A., and Cannon, A.: High-resolution meteorological forcing data for hydrological modelling and climate change impact analysis in the Mackenzie River Basin, Earth System Science Data, 12, 629–645, https://doi.org/10.5194/essd-12-629-2020, 2020.
- Betterle, A. and Bellin, A.: Morphological and Hydrogeological Controls of Groundwater Flows and Water Age Distribution in Mountain Aquifers and Streams, Water Resources Research, 60, e2024WR037407, https://doi.org/https://doi.org/10.1029/2024WR037407, e2024WR037407 2024WR037407, 2024.
 - Beven, K.: A manifesto for the equifinality thesis, Journal of Hydrology, 320, 18–36, https://doi.org/https://doi.org/10.1016/j.jhydrol.2005.07.007, the model parameter estimation experiment, 2006.
- Beven, K. J. and Binley, A. M.: The future of distributed models: Model calibration and uncertainty prediction, Hydrological Processes, 6, 279–298, https://doi.org/10.1002/hyp.3360060305, 1992.
 - Bierkens, M., Finke, P., and Willigen, P.: Upscaling and Downscaling Methods for Environmental Research, Dordrecht etc., Kluwer, 2000. Dev. Plant Soil Sci. 88, 190 pp, 88, 2001.
 - Birkel, C., Tetzlaff, D., and Dunn, S.: Towards a simple dynamic process conceptualization in rainfall-runoff models using multi-criteria calibration and tracers in temperate, upland catchments, Hydrological Processes, 24, 260 275, https://doi.org/10.1002/hyp.7478, 2009.
- Birkel, C., Soulsby, C., Tetzlaff, D., and Malcolm, I. A.: Modelling catchment-scale water storage dynamics: Reconciling dynamic storage with tracer-inferred passive storage, Hydrological Processes, 25, 3924–3936, https://doi.org/https://doi.org/10.1002/hyp.8201, 2011.
 - Birkel, C., Soulsby, C., Tetzlaff, D., and Dunn, S. M.: Developing a tracer-aided rainfall-runoff model to simulate hydrological processes in mesoscale catchments, Water Resources Research, 50, 944–961, https://doi.org/10.1002/2013WR014925, 2014.
- Birkel, C., Soulsby, C., and Tetzlaff, D.: Integrating parsimonious models of hydrological connectivity and soil biogeochemistry to simulate stream DOC dynamics, Water Resources Research, 51, 2541–2557, https://doi.org/https://doi.org/10.1002/2013JG002551, 2015.
 - Blasone, R.-S., Vrugt, J. A., Madsen, H., Rosbjerg, D., Robinson, B. A., and Zyvoloski, G. A.: Generalized likelihood uncertainty estimation (GLUE) using adaptive Markov Chain Monte Carlo sampling, Advances in Water Resources, 31, 630–648, https://doi.org/https://doi.org/10.1016/j.advwatres.2007.12.003, 2008.
 - Boral, S. and Sen, I. S.: Tracing 'Third Pole' ice meltwater contribution to the Himalayan rivers using oxygen and hydrogen isotopes, Geochemical Perspectives Letters, pp. 48–53, https://doi.org/10.7185/geochemlet.2013, 2020.
 - Borriero, A., Kumar, R., Nguyen, T. V., Fleckenstein, J. H., and Lutz, S. R.: Uncertainty in water transit time estimation with StorAge Selection functions and tracer data interpolation, Hydrology and Earth System Sciences, 27, 2989–3004, https://doi.org/10.5194/hess-27-2989-2023, 2023.

- Brazier, R. E., Beven, K. J., Freer, J., and Rowan, J. S.: Equifinality and uncertainty in physically based soil erosion models: application of the GLUE methodology to WEPP–the Water Erosion Prediction Project–for sites in the UK and USA, Earth Surface Processes and Landforms, 25, 825–845, https://doi.org/https://doi.org/10.1002/1096-9837(200008)25:8<825::AID-ESP101>3.0.CO;2-3, 2000.
 - Chang, Z., Gao, H., Yong, L., Wang, K., Chen, R., Han, C., Demberel, O., Dorjsuren, B., Hou, S., and Duan, Z.: Projected future changes in the cryosphere and hydrology of a mountainous catchment in the upper Heihe River, China, Hydrology and Earth System Sciences, 28, 3897–3917, https://doi.org/10.5194/hess-28-3897-2024, 2024.
- 635 Chen, J., Kuang, X., Fan, L., and Zheng, C.: Interbasin groundwater flows in the Yarlung Zangbo River Basin and its surrounding areas: A perspective, Science China-Technological Sciences, 68, https://doi.org/10.1007/s11431-024-2845-0, 2025.
 - Chen, X., Long, D., Hong, Y., Zeng, C., and Yan, D.: Improved modeling of snow and glacier melting by a progressive two-stage calibration strategy with GRACE and multisource data: How snow and glacier meltwater contributes to the runoff of the Upper Brahmaputra River basin?, Water Resources Research, 53, 2431–2466, https://doi.org/10.1002/2016wr019656, 2017.
- Chen, X., Long, D., Liang, S., He, L., Zeng, C., Hao, X., and Hong, Y.: Developing a composite daily snow cover extent record over the Tibetan Plateau from 1981 to 2016 using multisource data, Remote Sensing of Environment, 215, 284–299, https://doi.org/10.1016/j.rse.2018.06.021, 2018.

- Cui, T., Li, Y., Yang, L., Nan, Y., Li, K., Tudaji, M., Hu, H., Long, D., Shahid, M., Mubeen, A., He, Z., Yong, B., Lu, H., Li, C., Ni, G., Hu, C., and Tian, F.: Non-monotonic changes in Asian Water Towers' streamflow at increasing warming levels, NATURE COMMUNICATIONS, 14. https://doi.org/10.1038/s41467-023-36804-6. 2023.
- Dalla Torre, D., Di Marco, N., Menapace, A., Avesani, D., Righetti, M., and Majone, B.: Suitability of ERA5-Land reanalysis dataset for hydrological modelling in the Alpine region, Journal of Hydrology: Regional Studies, 52, 101718, https://doi.org/https://doi.org/10.1016/j.ejrh.2024.101718, 2024.
- Di Marco, N., Righetti, M., Avesani, D., Zaramella, M., Notarnicola, C., and Borga, M.: Comparison of MODIS and Model-Derived Snow-Covered Areas: Impact of Land Use and Solar Illumination Conditions, Geosciences, 10, https://doi.org/10.3390/geosciences10040134, 2020.
 - Di Marco, N., Avesani, D., Righetti, M., Zaramella, M., Majone, B., and Borga, M.: Reducing hydrological modelling uncertainty by using MODIS snow cover data and a topography-based distribution function snowmelt model, Journal of Hydrology, 599, 126 020, https://doi.org/https://doi.org/10.1016/j.jhydrol.2021.126020, 2021.
- 655 Didan, K.: MOD13A3 MODIS/Terra vegetation Indices Monthly L3 Global 1 km SIN Grid V006, https://doi.org/https://doi.org/10.5067/MODIS/MOD13A3.006, 2015.
 - Efstratiadis, A. and Koutsoyiannis, D.: One decade of multi-objective calibration approaches in hydrological modelling: a review, Hydrological Sciences Journal, 55, 58–78, https://doi.org/10.1080/02626660903526292, 2010.
- Fassnacht, S. R., Sexstone, G. A., Kashipazha, A. H., Ignacio Lopez-Moreno, J., Jasinski, M. F., Kampf, S. K., and Von Thaden, B. C.:

 Deriving snow-cover depletion curves for different spatial scales from remote sensing and snow telemetry data, HYDROLOGICAL PROCESSES, 30, 1708–1717, https://doi.org/10.1002/hyp.10730, 2016.
 - Fenicia, F., Kavetski, D., Reichert, P., and Albert, C.: Signature-Domain Calibration of Hydrological Models Using Approximate Bayesian Computation: Empirical Analysis of Fundamental Properties, Water Resources Research, 54, 3958–3987, https://doi.org/https://doi.org/10.1002/2017WR021616, 2018.

- Finger, D., Pellicciotti, F., Konz, M., Rimkus, S., and Burlando, P.: The value of glacier mass balance, satellite snow cover images, and hourly discharge for improving the performance of a physically based distributed hydrological model, Water Resources Research, https://doi.org/10.1029/2010WR009824, 2011.
 - Franks, S. W., Gineste, P., Beven, K. J., and Merot, P.: On constraining the predictions of a distributed model: The incorporation of fuzzy estimates of saturated areas into the calibration process, Water Resources Research, 34, 787–797, https://doi.org/https://doi.org/10.1029/97WR03041, 1998.
 - Gan, Y., Liang, X.-Z., Duan, Q., Ye, A., Di, Z., Hong, Y., and Li, J.: A systematic assessment and reduction of parametric uncertainties for a distributed hydrological model, Journal of Hydrology, 564, 697–711, https://doi.org/https://doi.org/10.1016/j.jhydrol.2018.07.055, 2018.
 - Gneiting, T., Balabdaoui, F., and Raftery, A. E.: Probabilistic forecasts, calibration and sharpness, Journal of the Royal Statistical Society: Series B (Statistical Methodology), 69, 243–268, https://doi.org/10.1111/j.1467-9868.2007.00587.x, 2007.
- 675 Grinsted, A.: An estimate of global glacier volume, CRYOSPHERE, 7, 141–151, https://doi.org/10.5194/tc-7-141-2013, 2013.

680

690

- Gupta, H., Wagener, T., and Liu, Y.: Reconciling Theory with Observations: Elements of a Diagnostic Approach to Model Evaluation, Hydrological Processes, 22, 3802 3813, https://doi.org/10.1002/hyp.6989, 2008.
- Hao, X., Huang, G., Zheng, Z., Sun, X., Ji, W., Zhao, H., Wang, J., Li, H., and Wang, X.: Development and validation of a new MODIS snow-cover-extent product over China, Hydrology and Earth System Sciences, 26, 1937–1952, https://doi.org/10.5194/hess-26-1937-2022, 2022.
- Haro-Monteagudo, D., Palazón, L., and Beguería, S.: Long-term sustainability of large water resource systems under climate change: A cascade modeling approach, Journal of Hydrology, 582, 124 546, https://doi.org/https://doi.org/10.1016/j.jhydrol.2020.124546, 2020.
- He, Y.: Pan-TPE soil map based on Harmonized World Soil Database (V1.2), https://data.tpdc.ac.cn/zh-hans/data/3519536a-d1e7-4ba1-8481-6a0b56637baf/?q=HWSD, 2019.
- 685 He, Z., Vorogushyn, S., Unger-Shayesteh, K., Gafurov, A., Kalashnikova, O., Omorova, E., and Merz, B.: The Value of Hydrograph Partitioning Curves for Calibrating Hydrological Models in Glacierized Basins, Water Resources Research, 54, 2336–2361, https://doi.org/https://doi.org/10.1002/2017WR021966, 2018.
 - He, Z., Unger-Shayesteh, K., Vorogushyn, S., Weise, S. M., Kalashnikova, O., Gafurov, A., Duethmann, D., Barandun, M., and Merz, B.: Constraining hydrological model parameters using water isotopic compositions in a glacierized basin, Central Asia, Journal of Hydrology, 571, 332–348, https://doi.org/10.1016/j.jhydrol.2019.01.048, 2019.
 - He, Z., Duethmann, D., and Tian, F.: A meta-analysis based review of quantifying the contributions of runoff components to streamflow in glacierized basins, Journal of Hydrology, 603, 126 890, https://doi.org/10.1016/j.jhydrol.2021.126890, 2021.
 - Hindshaw, R. S., Tipper, E. T., Reynolds, B. C., Lemarchand, E., Wiederhold, J. G., Magnusson, J., Bernasconi, S. M., Kretzschmar, R., and Bourdon, B.: Hydrological control of stream water chemistry in a glacial catchment (Damma Glacier, Switzerland), CHEMICAL GEOLOGY, 285, 215–230, https://doi.org/10.1016/j.chemgeo.2011.04.012, 2011.
 - Hugonnet, R., McNabb, R., Berthier, E., Menounos, B., Nuth, C., Girod, L., Farinotti, D., Huss, M., Dussaillant, I., Brun, F., and Kaab, A.: Accelerated global glacier mass loss in the early twenty-first century, Nature, 592, 726—+, https://doi.org/10.1038/s41586-021-03436-z, 2021.
- Huss, M. and Hock, R.: A new model for global glacier change and sea-level rise, Frontiers in Earth Science, 3, https://doi.org/10.3389/feart.2015.00054, 2015.
 - Jasechko, S.: Global Isotope Hydrogeology—Review, Reviews of Geophysics, 57, 835–965, https://doi.org/https://doi.org/10.1029/2018RG000627, 2019.

- Jasechko, S. and Taylor, R.: Intensive rainfall recharges tropical groundwaters, Environmental Research Letters, 10, 124 015, https://doi.org/10.1088/1748-9326/10/12/124015, 2015.
- Jiang, Y., Yang, K., Yang, H., Lu, H., Chen, Y., Zhou, X., Sun, J., Yang, Y., and Wang, Y.: Characterizing basin-scale precipitation gradients in the Third Pole region using a high-resolution atmospheric simulation-based dataset, Hydrology Earth System Sciences, 26, 4587–4601, https://doi.org/10.5194/hess-26-4587-2022, 2022.
 - Jin, X., Xu, C. Y., Zhang, Q., and Singh, V.: Parameter and modeling uncertainty simulated by GLUE and a formal Bayesian method for a conceptual hydrological model, Journal of Hydrology, 383, 147–155, https://doi.org/https://doi.org/10.1016/j.jhydrol.2009.12.028, 2010.
- Khanal, S., Lutz, A. F., Kraaijenbrink, P. D. A., van den Hurk, B., Yao, T., and Immerzeel, W. W.: Variable 21st Century Climate Change Response for Rivers in High Mountain Asia at Seasonal to Decadal Time Scales, Water Resources Research, 57, https://doi.org/10.1029/2020wr029266, 2021.
 - Lamontagne, J. and Barber, C.: Improved Estimators of Model Performance Efficiency for Skewed Hydrologic Data, Water Resources Research, 56, https://doi.org/10.1029/2020WR027101, 2020.
- Lin, J., Bryan, B. A., Zhou, X., Lin, P., Do, H. X., Gao, L., Gu, X., Liu, Z., Wan, L., Tong, S., Huang, J., Wang, Q., Zhang, Y., Gao, H., Yin, J., Chen, Z., Duan, W., Xie, Z., Cui, T., Liu, J., Li, M., Li, X., Xu, Z., Guo, F., Shu, L., Li, B., Zhang, J., Zhang, P., Fan, B., Wang, Y., Zhang, Y., Huang, J., Li, X., Cai, Y., and Yang, Z.: Making China's water data accessible, usable and shareable, Nature Water, 1, 328–335, https://doi.org/10.1038/s44221-023-00039-y, 2023.
 - Liu, S.: The second glacier inventory dataset of China (version 1.0) (2006–2011), https://doi.org/10.3972/glacier.001.2013.db, 2012.
- 720 Lutz, A. F., Immerzeel, W. W., Shrestha, A. B., and Bierkens, M. F. P.: Consistent increase in High Asia's runoff due to increasing glacier melt and precipitation, Nature Climate Change, 4, 587–592, https://doi.org/10.1038/nclimate2237, 2014.
 - Lutz, A. F., Immerzeel, W. W., Kraaijenbrink, P. D. A., Shrestha, A. B., and Bierkens, M. F. P.: Climate Change Impacts on the Upper Indus Hydrology: Sources, Shifts and Extremes, Plos One, 11, https://doi.org/10.1371/journal.pone.0165630, 2016.
- Ma, J., Li, R., Zheng, H., Li, W., Rao, K., Yang, Y., and Wu, B.: Multivariate adaptive regression splines-assisted approximate Bayesian computation for calibration of complex hydrological models, Journal of Hydroinformatics, 26, 503–518, https://doi.org/10.2166/hydro.2024.232, 2024.
 - Majone, B., Avesani, D., Zulian, P., Fiori, A., and Bellin, A.: Analysis of high streamflow extremes in climate change studies: how do we calibrate hydrological models?, Hydrology and Earth System Sciences, 26, 3863–3883, https://doi.org/10.5194/hess-26-3863-2022, 2022.
 - McGuire, K. J. and McDonnell, J. J.: A review and evaluation of catchment transit time modeling, Journal of Hydrology, 330, 543–563, 2006.

- McKay, M. D., Beckman, R. J., and Conover, W. J.: A Comparison of Three Methods for Selecting Values of Input Variables in the Analysis of Output from a Computer Code, Technometrics, 21, 239–245, http://www.jstor.org/stable/1268522, 1979.
- Mohammadi, B., Gao, H., Feng, Z., Pilesjö, P., Cheraghalizadeh, M., and Duan, Z.: Simulating Glacier Mass Balance and its Contribution to Runoff in Northern Sweden, Journal of Hydrology, 620, https://doi.org/10.1016/j.jhydrol.2023.129404, 2023.
- Molotch, N. P. and Margulis, S. A.: Estimating the distribution of snow water equivalent using remotely sensed snow cover data and a spatially distributed snowmelt model: A multi-resolution, multi-sensor comparison, Advances in Water Resources, 31, 1503–1514, https://doi.org/https://doi.org/10.1016/j.advwatres.2008.07.017, hydrologic Remote Sensing, 2008.
 - Moriasi, D., Arnold, J., Van Liew, M., Bingner, R., Harmel, R., and Veith, T.: Model Evaluation Guidelines for Systematic Quantification of Accuracy in Watershed Simulations, Transactions of the ASABE, 50, https://doi.org/10.13031/2013.23153, 2007.

- Muñoz-Sabater, J., Dutra, E., Agustí-Panareda, A., Albergel, C., Arduini, G., Balsamo, G., Boussetta, S., Choulga, M., Harrigan, S., Hersbach, H., et al.: ERA5-Land: A state-of-the-art global reanalysis dataset for land applications, Earth system science data, 13, 4349–4383, https://doi.org/10.5194/essd-13-4349-2021, 2021.
 - Myneni, R., Knyazikhin, Y., and Park, T.: MOD15A2H MODIS/Terra Leaf Area Index/FPAR 8-Day L4 Global 500 m SIN Grid V006, https://doi.org/10.5067/MODIS/MOD15A2H.006, 2015.
- Nan, Y. and Tian, F.: Isotope data-constrained hydrological model improves soil moisture simulation and runoff source apportionment, Journal of Hydrology, 633, 131 006, https://doi.org/https://doi.org/10.1016/j.jhydrol.2024.131006, 2024.
 - Nan, Y., He, Z., Tian, F., Wei, Z., and Tian, L.: Can we use precipitation isotope outputs of isotopic general circulation models to improve hydrological modeling in large mountainous catchments on the Tibetan Plateau?, Hydrology and Earth System Sciences, 25, 6151–6172, 2021a.
- Nan, Y., Tian, L., He, Z., Tian, F., and Shao, L.: The value of water isotope data on improving process understanding in a glacierized catchment on the Tibetan Plateau, Hydrology and Earth System Sciences, 25, 3653–3673, 2021b.
 - Nan, Y., He, Z., Tian, F., Wei, Z., and Tian, L.: Assessing the influence of water sampling strategy on the performance of tracer-aided hydrological modeling in a mountainous basin on the Tibetan Plateau, HYDROLOGY AND EARTH SYSTEM SCIENCES, 26, 4147–4167, https://doi.org/10.5194/hess-26-4147-2022, 2022.
- Nan, Y., Tian, F., Li, Z., and Gui, J.: Longer simulation time step of the tracer-aided hydrological model estimates lower contribution of slow runoff components, Journal of Hydrology, pp. 129 889–129 889, https://doi.org/10.1016/j.jhydrol.2023.129889, 2023.
 - Nan, Y., Tian, F., and Li, Z.: Model Diagnostic Analysis in a Cold Basin Influenced by Frozen Soils With the Aid of Stable Isotope, WATER RESOURCES RESEARCH, 60, https://doi.org/10.1029/2024WR037218, 2024.
- Nan, Y., Tian, F., McDonnell, J., Ni, G., Tian, L., Li, Z., Yan, D., Xia, X., Wang, T., Han, S., and Li, K.: Glacier meltwater has limited contributions to the total runoff in the major rivers draining the Tibetan Plateau, Npj Climate and Atmospheric Science, 8, https://doi.org/10.1038/s41612-025-01060-6, 2025.
 - Nash, J. and Sutcliffe, J.: River flow forecasting through conceptual models part I A discussion of principles, Journal of Hydrology, 10, 282–290, https://doi.org/10.1016/0022-1694(70)90255-6, 1970.
- O'Neel, S., Hood, E., Arendt, A., and Sass, L.: Assessing streamflow sensitivity to variations in glacier mass balance, Climatic Change, 123, 329–341, https://doi.org/10.1007/s10584-013-1042-7, 2014.
 - Panchanathan, A., Ahrari, A., Ghag, K. S., Mustafa, S., Haghighi, A. T., Kløve, B., and Oussalah, M.: An overview of approaches for reducing uncertainties in hydrological forecasting: Progress and challenges, Earth-Science Reviews, 258, 104956, https://doi.org/10.1016/j.earscirev.2024.104956, 2024.
- Raleigh, M. S., Lundquist, J. D., and Clark, M. P.: Exploring the impact of forcing error characteristics on physically based snow simulations within a global sensitivity analysis framework, Hydrology and Earth System Sciences, 19, 3153–3179, https://doi.org/10.5194/hess-19-3153-2015, 2015.
 - Reggiani, P., Hassanizadeh, S., Sivapalan, M., and Gray, W. G.: A unifying framework for watershed thermodynamics: constitutive relationships, Advances in Water Resources, 23, 15–39, https://doi.org/10.1016/S0309-1708(99)00005-6, 1999.
- Rodgers, P., Soulsby, C., Waldron, S., and Tetzlaff, D.: Using stable isotope tracers to assess hydrological flow paths, residence times and landscape influences in a nested mesoscale catchment, Hydrology and Earth System Sciences, 9, 139–155, https://doi.org/10.5194/hess-9-139-2005, 2005.

- Ruelland, D.: Potential of snow data to improve the consistency and robustness of a semi-distributed hydrological model using the SAFRAN input dataset, Journal of Hydrology, 631, 130 820, https://doi.org/https://doi.org/10.1016/j.jhydrol.2024.130820, 2024.
- Shuai, P., Chen, X., Mital, U., Coon, E. T., and Dwivedi, D.: The effects of spatial and temporal resolution of gridded meteorological forcing on watershed hydrological responses, Hydrology and Earth System Sciences, 26, 2245–2276, https://doi.org/10.5194/hess-26-2245-2022, 2022.
 - Stahl, K., Moore, R. D., Shea, J. M., Hutchinson, D., and Cannon, A. J.: Coupled modelling of glacier and streamflow response to future climate scenarios, Water Resources Research, 44, https://doi.org/https://doi.org/10.1029/2007WR005956, 2008.
- Sun, H., Yao, T. D., Su, F. G., Yang, W., and Chen, D. L.: Spatiotemporal responses of runoff to climate change in the southern Tibetan Plateau, Hydrology and Earth System Sciences, 28, 4361–4381, https://doi.org/10.5194/hess-28-4361-2024, 2024.
 - Tetzlaff, D., Birkel, C., Dick, J., and Geris, J.: Storage dynamics in hydropedological units control hillslope connectivity, runoff generation, and the evolution of catchment transit time distributions, Water resources research, 50, 969–985, https://doi.org/10.1002/2013WR014147, 2014.
- Teweldebrhan, A. T., Burkhart, J. F., and Schuler, T. V.: Parameter uncertainty analysis for an operational hydrological model using residual-based and limits of acceptability approaches, Hydrology and Earth System Sciences, 22, 5021–5039, https://doi.org/10.5194/hess-22-5021-2018, 2018.
 - Tian, F., Hu, H., Lei, Z., and Sivapalan, M.: Extension of the Representative Elementary Watershed approach for cold regions via explicit treatment of energy related processes, Hydrology and Earth System Sciences, 10, 619–644, https://doi.org/10.5194/hess-10-619-2006, 2006.
- Tong, R., Parajka, J., Salentinig, A., Pfeil, I., Komma, J., Széles, B., Kubáň, M., Valent, P., Vreugdenhil, M., Wagner, W., and Blöschl, G.:

 The value of ASCAT soil moisture and MODIS snow cover data for calibrating a conceptual hydrologic model, Hydrology and Earth System Sciences, 25, 1389–1410, https://doi.org/10.5194/hess-25-1389-2021, 2021.

- Tong, R., Parajka, J., Széles, B., Greimeister-Pfeil, I., Vreugdenhil, M., Komma, J., Valent, P., and Blöschl, G.: The value of satellite soil moisture and snow cover data for the transfer of hydrological model parameters to ungauged sites, Hydrology and Earth System Sciences, 26, 1779–1799, https://doi.org/10.5194/hess-26-1779-2022, 2022.
- Wu, Y., Sun, J., Blanchette, M., Rousseau, A. N., Xu, Y. J., Hu, B., and Zhang, G.: Wetland mitigation functions on hydrological droughts: From drought characteristics to propagation of meteorological droughts to hydrological droughts, Journal of Hydrology, 617, 128 971, https://doi.org/https://doi.org/10.1016/j.jhydrol.2022.128971, 2023.
- Xu, M., Yan, M., Kang, J., and Ren, J.: Comparative studies of glacier mass balance and their climatic implications in Svalbard, Northern Scandinavia, and Southern Norway, Environmental Earth Sciences, 67, 1407–1414, https://doi.org/10.1007/s12665-012-1585-3, 2012.
- Xu, R., Tian, F., Yang, L., Hu, H., Lu, H., and Hou, A.: Ground validation of GPM IMERG and TRMM 3B42V7 rainfall products over southern Tibetan Plateau based on a high-density rain gauge network, Journal of Geophysical Research: Atmospheres, 122, 910–924, https://doi.org/10.1002/2016JD025418, 2017.
- Yang, J., Reichert, P., and Abbaspour, K. C.: Bayesian uncertainty analysis in distributed hydrologic modeling: A case study in the Thur River basin (Switzerland), Water Resources Research, 43, https://doi.org/https://doi.org/10.1029/2006WR005497, 2007.
 - Yang, K. and He, J.: China meteorological forcing dataset (1979-2018), https://doi.org/10.11888/AtmosphericPhysics.tpe.249369.file, 2019.
 - Yang, L., Feng, Q., Ning, T., Lu, T., Zhu, M., Yin, X., and Wang, J.: Attributing the streamflow variation by incorporating glacier mass balance and frozen ground into the Budyko framework in alpine rivers, Journal of Hydrology, 628, 130438, https://doi.org/https://doi.org/10.1016/j.jhydrol.2023.130438, 2024.

- Yoshimura, K., Kanamitsu, M., Noone, D., and Oki, T.: Historical isotope simulation using Reanalysis atmospheric data, Journal of Geophysical Research-Atmospheres, 113, https://doi.org/10.1029/2008jd010074, 2008.
 - Zhang, M. J., Nan, Y., and Tian, F. Q.: Runoff component quantification and future streamflow projection in a large mountainous basin based on a multidata-constrained cryospheric-hydrological model, Hydrology and Earth System Sciences, 29, 1033–1060, https://doi.org/10.5194/hess-29-1033-2025, 2025.
- 820 Zhang, Q., Knowles, J. F., Barnes, R. T., Cowie, R. M., Rock, N., and Williams, M. W.: Surface and subsurface water contributions to streamflow from a mesoscale watershed in complex mountain terrain, Hydrological Processes, 32, 954–967, https://doi.org/10.1002/hyp.11469, 2018.